J Mol Model (2012) 18:4171–4189
DOI 10.1007/s00894-012-1406-3

ORIGINAL PAPER

Structures, energies and bonding in neutral and charged Li microclusters

Diana Yepes · Steven Robert Kirk · Samantha Jenkins · Albeiro Restrepo

Received: 16 January 2012 / Accepted: 8 March 2012 / Published online: 27 April 2012

Abstract Structural and chemical properties of charged and neutral Lithium microclusters are investigated for $Li_n^q (n = 5-10, q = 0, \pm 1)$. A total of 18 quantum conformational spaces are randomly walked to produce candidate structures for local minima. Very rich potential energy surfaces are produced, with the largest structural complexity predicted for anionic clusters. Analysis of the electron charge distributions using the quantum theory of atoms in molecules (QTAIM) predicts major stabilizing roles of Non–nuclear attractors (NNAs) via NNA···Li interactions with virtually no direct Li···Li interactions, except in the least stable configurations. A transition in behavior for clusters containing more than seven nuclei is observed by using the recently introduced quantum topology to determine in a quantum mechanically consistent fashion the number of spatial dimensions each cluster has. We experiment with a novel scheme for extracting persistent structural motifs with increase in cluster size. The new structural motifs correlate well with the energetic stability, particularly in highlighting the least stable structures. Quantifying the degree of covalent character in Lithium bonding independently agrees with the observation in the transition in cluster behavior for lithium clusters containing more than seven nuclei. Good correlation with available experimental data is obtained for all properties reported in this work.

Keywords Cluster growth · Lithium microclusters · QTAIM · Stochastic optimization

Electronic supplementary material The online version of this article (doi:10.1007/s00894-012-1406-3) contains supplementary material, which is available to authorized users.

D. Yepes
Departamento de Ciencias Químicas, Facultad de Ciencias Exactas, Universidad Andres Bello,
Avenida República 275,
8370146 Santiago, Chile

S. R. Kirk · S. Jenkins (✉)
College of Chemistry and Chemical Engineering,
Hunan Normal University,
Changsha, Hunan 410081, China
e-mail: suman@hunnu.edu.cn

A. Restrepo (✉)
Grupo de Química–Física Teórica, Instituto de Química,
Universidad de Antioquia,
AA 1226 Medellín, Colombia
e-mail: albeiro@matematicas.udea.edu.co

Introduction

Vasts amounts of scientific literature are routinely devoted to the study of clusters. Current understanding of nature at the atomic, molecular levels as well as at the macroscopic level is way more complete than knowledge in the cluster regime, clusters properties and behavior representing a transition from atoms and molecules to bulk matter. The chief obstacle preventing deeper insights into clusters is the fact that their properties change by the addition or removal of individual atoms or molecules.

Lithium clusters, Li_n, have been extensively studied, among other reasons, because having three electrons, Li atoms are the smallest that can form metallic clusters under normal conditions (hydrogen atom clusters are known to become metallic under extreme pressures). Experimentally measured properties for lithium clusters include ionization potentials (IPs), [1] electron affinities (EAs), [2] polarizabilities, [3] cohesive energies [4] and others. Recently, small anionic lithium clusters, $Li_n^- - (n = 3-7)$ have been investigated via a combination of photoelectron spectroscopy and *ab initio* calculations [2]. Among the large variety of theoretical methods used to study lithium clusters, we cite several flavors of DFT [5–11], configuration interaction [9, 12–15], MP2 [9, 11, 16], coupled clusters [5, 9, 11, 17,

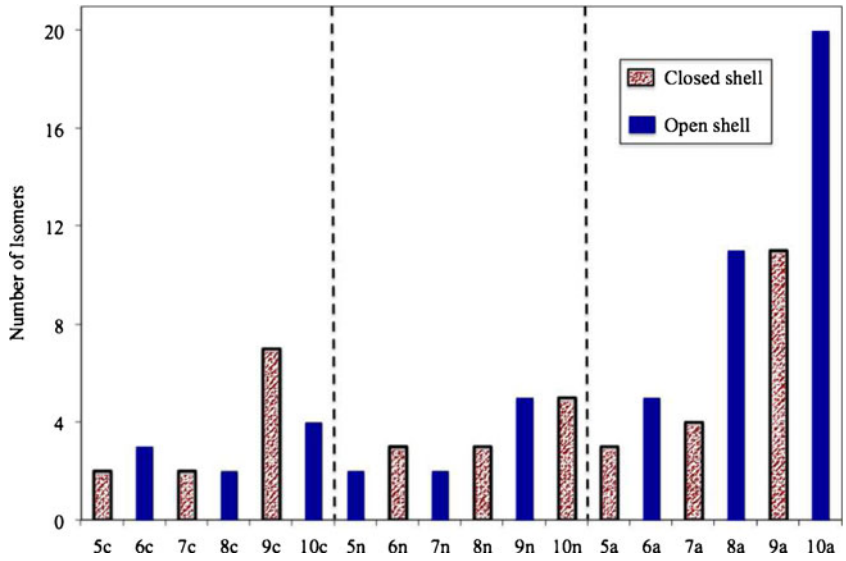

Fig. 1 Number of isomers for each conformational space in Li_n^q clusters classified as either closed or open shell (pointed and solid bars respectively). The vertical dashed lines separate the systems according to their charge: cations, neutrals and anions

18], CASSCF [9], generalized valence bond theory [19–21], *ab initio* molecular dynamics [22], *ab initio* path integral methods [9, 23, 24], variational quantum Monte Carlo methods [25], and gradient embedded genetic algorithms [5]. Several works have shown that electron correlation energy is an essential contribution to cluster stability [11–13, 26–28]. Boustani and Koutecký determined that geometries for anionic lithium clusters differ appreciably from those in neutral and cationic clusters [29].

Chemical bonding in Li_n has been discussed from molecular orbital analysis by Alexandrova and Boldyrev, they concluded that multiple π and σ aromaticity play significant roles as major stabilizing effects [5]. Visser and coworkers reported that high spin lithium clusters, despite having no bonding electron pairs, exhibit rich conformational spaces, with clusters being held together via multiplet interactions [30]. Pérez and coworkers have provided the most exhaustive characterization of the potential energy surfaces (PESs) for $Li_{5,6,7}^{0,\pm1}$ microclusters in their lowest spin states at the MP2 level [11]. Regarding structural issues, for homonuclear metallic clusters M_n, n=6 seems to be the transition point from planar (n<6) to 3D (n>6) structural preference [11, 17, 31, 32]; exceptions to this rule are known, for example, planar geometries for cationic, neutral and anionic Au_{12} clusters are reported as the most stable [33–36]. Relativistic effects have been postulated to be responsible for such "anomalous" structural preferences [37]. Interestingly, n=6 is also the transition point from planar to 3D preferred geometries in water clusters [38]. An explanation for such structural preferences has been recently provided [39] by means of the quantum theory of atoms in molecules (QTAIM), it involves the identification of cage critical points (CCPs) only for $n \geq 6$. Jenkins and

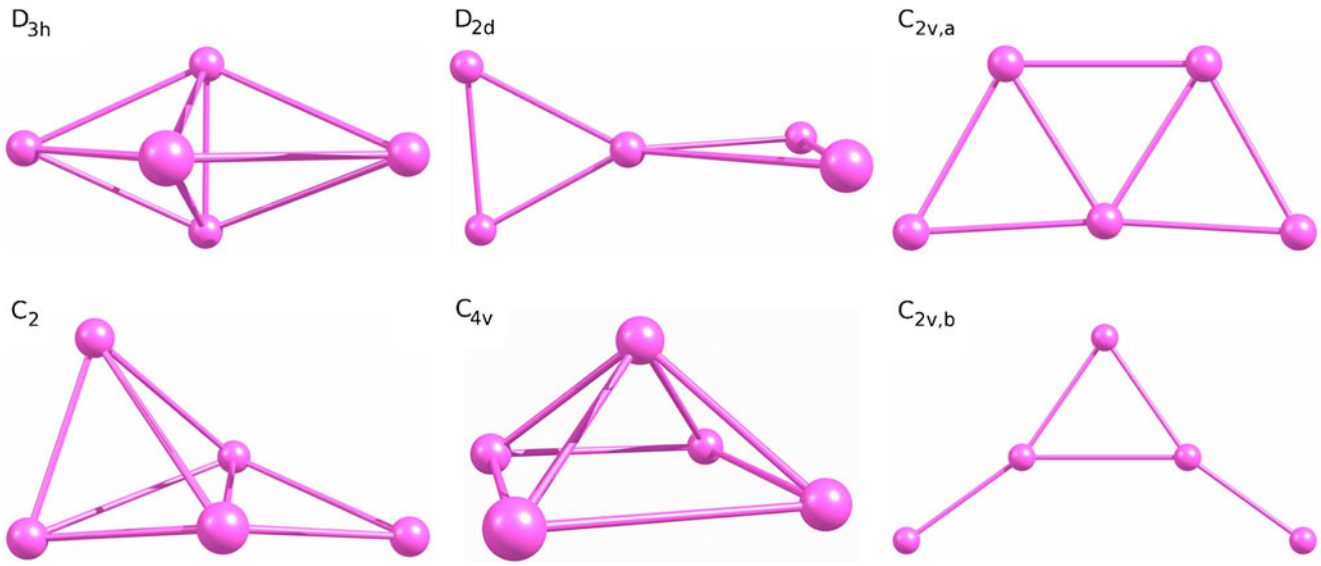

Fig. 2 Geometrical motifs for neutral and charged Li_5 clusters. Lines joining atoms are drawn to help visualize the geometrical motifs

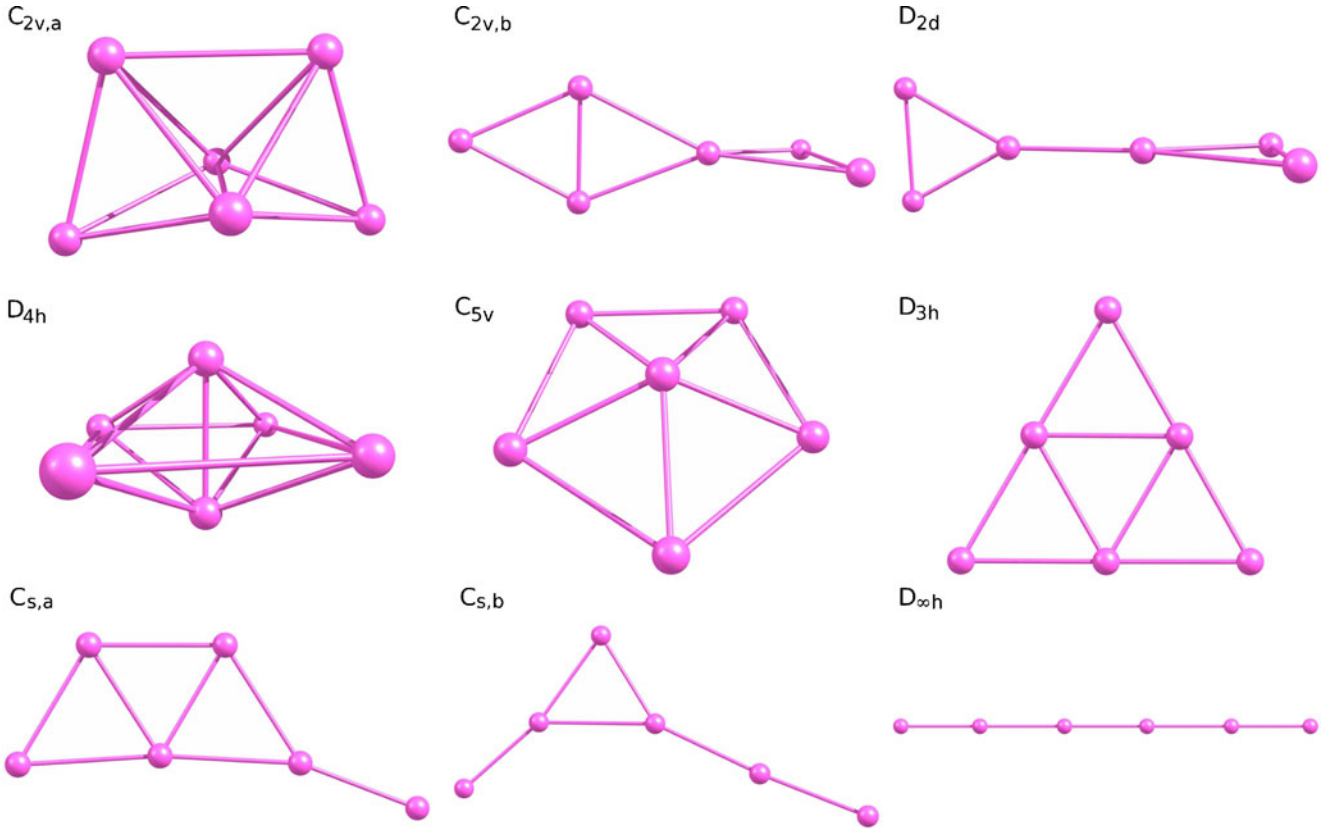

Fig. 3 Geometrical motifs for neutral and charged Li_6 clusters. Lines joining atoms are drawn to help visualize the geometrical motifs

coworkers suggested in the same work that dimensionality of molecular geometries should be achieved via quantum topological analysis of the electron densities, since the rules of euclidean geometry should not be applied at the molecular scale to describe molecular structures. In this context, the existence of only bond critical points (BCPs) will characterize a structure as 1D in the quantum topological (QT) sense regardless of the disposition of atoms; at least one ring critical point (RCP) would lead to 2D QT structures, while CCPs would characterize a structure as 3D according to quantum topology.

Conformational spaces for alkali–metal clusters are notoriously difficult to characterize because the presence of only one *s* electron in the valence shells leads to very flat potential energy surfaces (PESs), numerous shallow local minima appearing because of the non–directional bonding [17]. A problematic issue in the study of atomic and molecular clusters is the generation of equilibrium structures. Modern advances in technology produce fast and powerful computers that have allowed the recent implementation of stochastic optimization methods with energy evaluated via quantum Hamiltonians [5, 40–43]. In particular, a modified Metropolis acceptance test in the simulated annealing optimization procedure [44–46] has recently been proposed [11, 47, 48] as means for generating cluster candidate structures that undergo further optimizations by traditional gradient following techniques. The method, incorporated into the ASCEC (after its Spanish acronym Annealing Simulado Con Energía Cuántica) program, [48] retains the comparative advantages and disadvantages of stochastic optimization over analytical

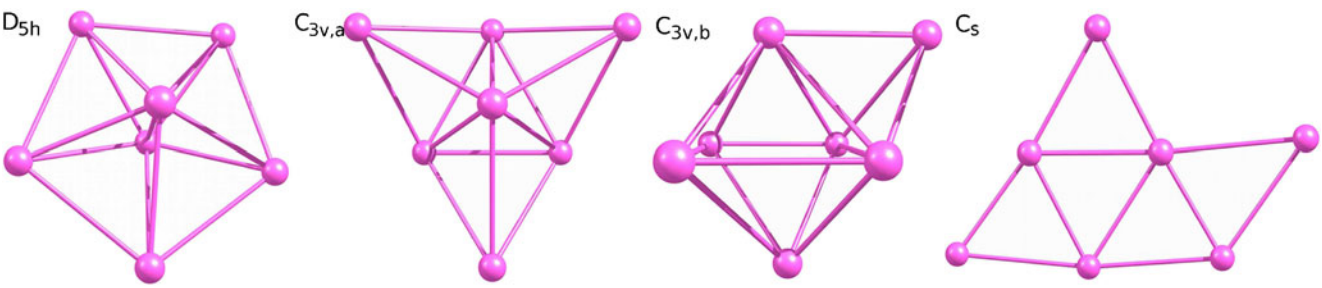

Fig. 4 Geometrical motifs for neutral and charged Li_7 clusters. Lines joining atoms are drawn to help visualize the geometrical motifs

methods, [49] namely, initial guess independence, exhaustive exploration of the potential energy surface, and the ability to jump over energy barriers and to sample several energy wells on the same run without getting trapped in local minima; however, the method is still computationally intensive because of repetitive evaluation of the energy function. The ASCEC method has been successfully used to treat mono and bimetallic atomic microclusters [11, 50], molecular clusters joint via hydrogen bonding networks, [38, 39, 47, 51–53] and mixed atoms/molecules clusters [54] stabilized via a wide variety of complex interactions. The studies in question afforded contributing new structures never before reported in the literature, which in the proper cases have helped rationalizing the stabilization of small hydrogen–bonded networks, the reactivity of metallic microclusters and the nature and complex interplay between forces involved in the microsolvation of alkali metal cations.

In this work, we undertake a systematic exploration of the conformational spaces of $Li_n^q (n = 5-10, q = 0, \pm 1)$ microclusters in their lowest spin states. A study with the same methodology of the n=5−7 clusters can be found elsewhere [11]; those results are also included in this report for the sake of completeness, to elaborate trends, to draw conclusions based in larger samples, and because of new analysis not included in the previous manuscript. We aim at expanding the limited knowledge of these very important PESs as well as at shedding light into the nature of interactions responsible for cluster stabilization and bonding.

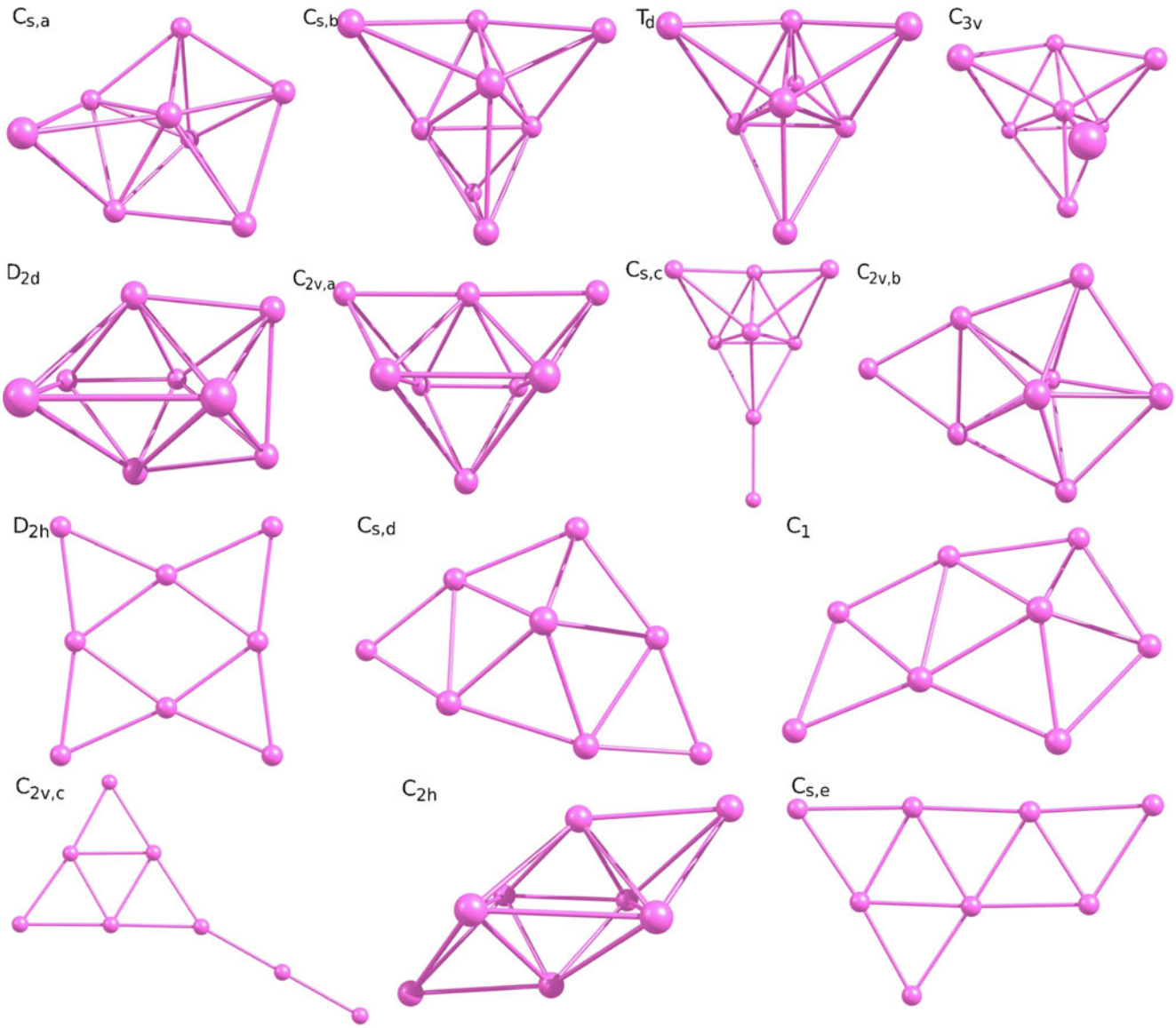

Fig. 5 Geometrical motifs for neutral and charged Li_8 clusters. Lines joining atoms are drawn to help visualize the geometrical motifs

Computer methods and theory

We used the molecular cluster capabilities of the ASCEC program [48] which contains a modified Metropolis acceptance test in an adapted version of the simulated annealing optimization procedure. The annealing algorithm [44–46] was used to generate candidate structures after random walks of the HF/lanl2dz PESs. The BLYP density functional in conjunction with the 6–311+G(d) basis set was used to optimize and characterize the structures afforded by ASCEC. Further refinement and characterization of the located minima was conducted by means of B3LYP/6–311+G(d) calculations. Analytical harmonic second derivative calculations were used to characterize all stationary points as true minima (no negative eigenvalues of the Hessian matrix). Highly correlated CCSD(T)/6–311+G(d) energies were calculated on all B3LYP optimized geometries. This choice of methodology has proven very successful in the treatment of $Li_{5,6,7}^{0,\pm1}$ clusters [11].

Binding energies (BE) were calculated by subtracting the energy of the given cluster from the sum of the energies of the constituent atoms, in this way, larger positive numbers correspond to larger stabilization energies. Relative energies (ΔE) were calculated as the difference between the energy of the most stable structure and the energy of a particular cluster on a given PES. Isomer populations were estimated by standard Boltzmann distribution analysis using both the ZPE corrected B3LYP and CCSD(T)//B3LYP calculated energies. Adiabatic ionization potentials were estimated as the difference between the statistically weighted average

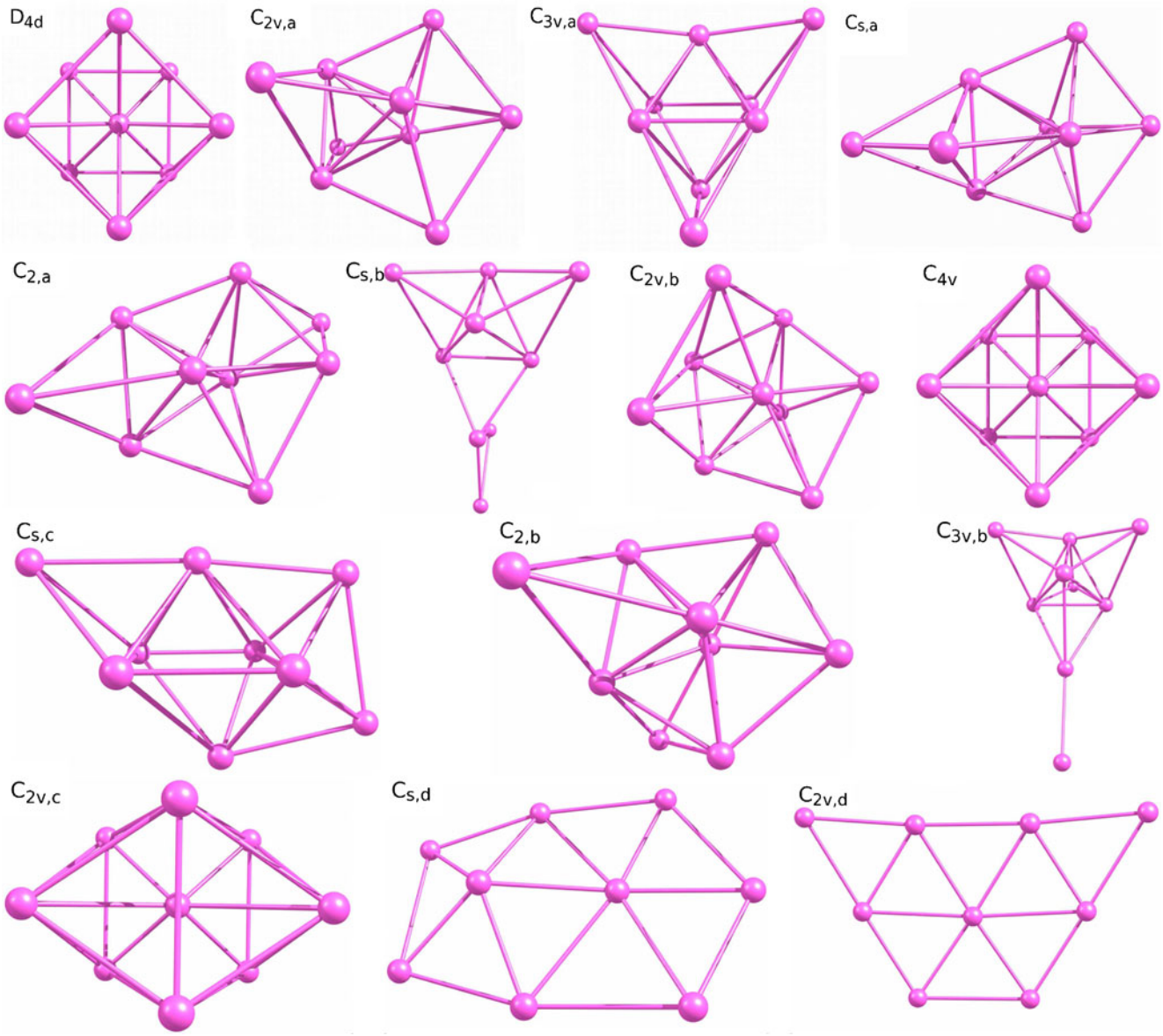

Fig. 6 Geometrical motifs for neutral and charged Li_9 clusters. Lines joining atoms are drawn to help visualize the geometrical motifs

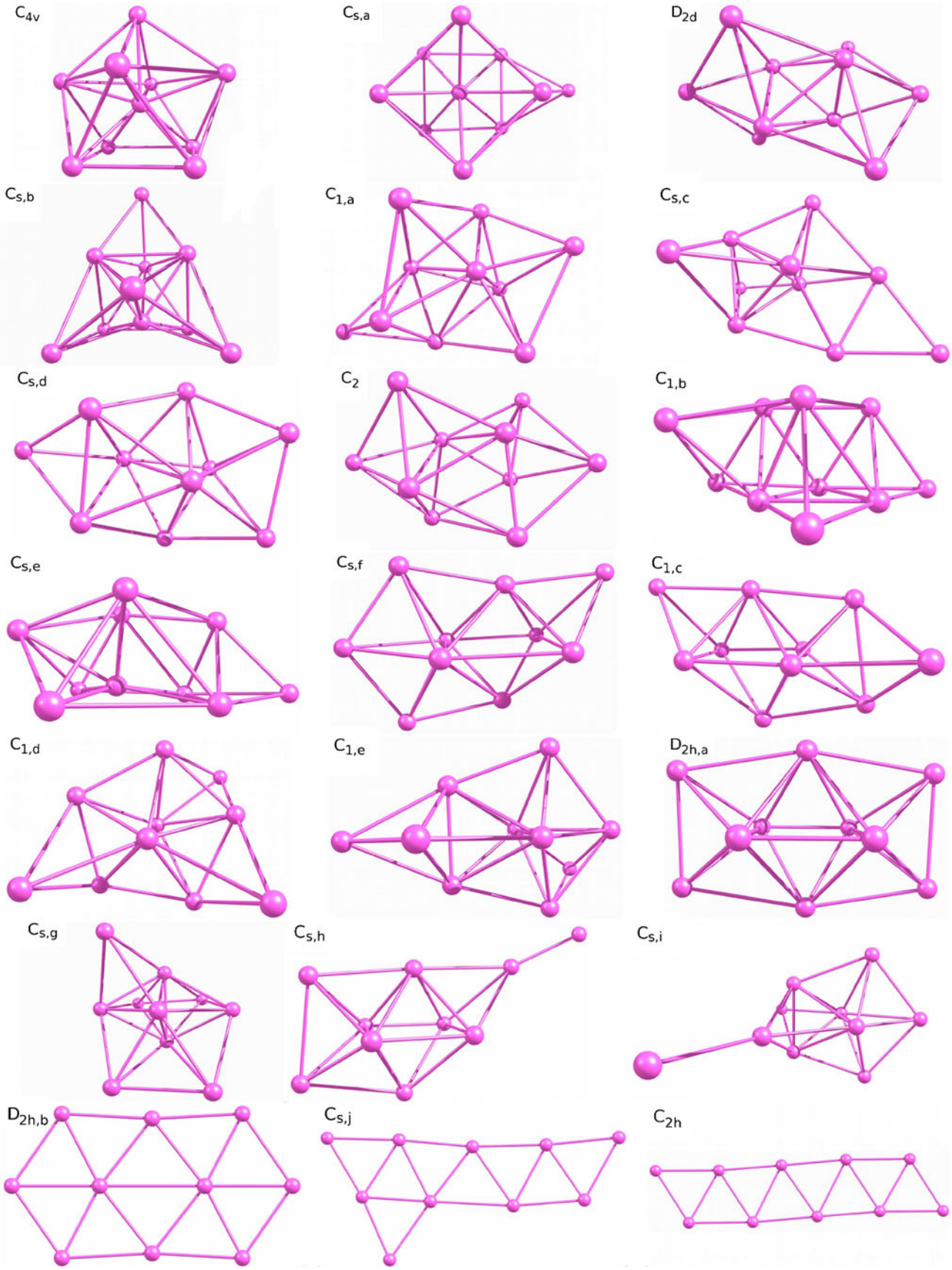

Fig. 7 Geometrical motifs for neutral and charged Li_{10} clusters. Lines joining a toms are drawn to help visualize the geometrical motifs

energies of the neutral clusters and the statistically weighted average energies of the cationic structures for a given number of Li atoms, the weighting factor taken as the estimated Boltzmann populations. All optimization, frequency, and energy calculations were carried out using the Gaussian 03 suite of programs [55].

The properties of the electronic charge distributions for Li_n^q clusters are analyzed in the context of the quantum theory of atoms in molecules, QTAIM [56]. QTAIM defines an atom as an open system and provides a powerful method for the study of bonding using only the charge density distribution ρ (**r**). Within QTAIM, critical points in the charge density distribution are identified where $\nabla\rho$ (**r**)=0, and further classified according to the properties of the Hessian matrix (the matrix of partial second derivatives of **F**(**r**) with respect to the components of **r**) evaluated at these points. Diagonalizing this matrix gives the coordinate invariant (ordered) eigenvalues $\lambda_1<\lambda_2<\lambda_3$; the critical points are conventionally labeled using the notation (ω , σ) where ω is the rank (the number of distinct eigenvalues) and σ is the signature (the algebraic sum of the signs of the eigenvalues).

In three dimensions, there are five types of topologically stable critical points, these are denoted as (3,-3), which are local maxima, usually corresponding to a nuclear position (NCP), in this work we also include non–nuclear maxima (NNA); other critical points are (3,-1) and (3,+1), which correspond to saddle points, called bond critical points (BCP) and ring critical points (RCP), respectively; finally, there are also (3,+3), cage critical points (CCP).

We are interested in properties evaluated at the BCPs, RCPs, and CCPs, e.g., the charge density evaluated at the BCP denoted by ρ ($\mathbf{r}_b$), its Laplacian $\nabla^2\rho$ ($\mathbf{r}_b$), and the local total energy $\mathscr{H}$ ($\mathbf{r}_b$), also evaluated at the BCP. Closed shell interactions (e.g., ionic bonds, hydrogen bonds, non–bonding interactions) are characterized by positive values of the Laplacian, $\nabla^2\rho$ ($\mathbf{r}_b$), low ρ ($\mathbf{r}_b$) values (<0.1 atomic units), and values of $|\lambda_1|$ /$\lambda_3<1$; these types of interactions are dominated by the contraction of charge away from the BCP toward each of the nuclei. Conversely, shared interactions (e.g., covalent bonds) have negative $\nabla^2\rho$ ($\mathbf{r}_b$) values, high values of ρ ($\mathbf{r}_b$), and values of $|\lambda 1|$ /$\lambda 3>1$. For a given molecular system, the numbers of the four different types of critical points are related by a fundamental theorem of topology, the Poincaré–Hopf relationship [56]:

$$n - b + r - c = 1, \quad (1)$$

where n, b, r, and c are the numbers of NCPs BCPs, RCPs, and CCPs, respectively. When we are considering systems with flat regions of charge density then there are also naturally arising maxima: Non–nuclear attractors (NNAs) which are included into the total for n within Eq. 1, but unlike the number of NCPs for a given cluster size, the number of NNAs can change for given cluster sizes.

In this work we will use the recently introduced concept of quantum topology within QTAIM instead of using Euclidean geometry to determine whether a structure is 3D, 2D or 1D, [39] the following notation is used to refer to all possible molecular geometries consistent with

Table 1 Energetic analysis for the $Li_{5,6,7}^{0,\pm1}$ clusters. ΔE: Relative energies with respect to the most stable structure within a given PES at each level. BE/atom: Binding energies/atom. All relative and binding energies corrected for the unscaled corresponding ZPEs. CCSD(T) energies corrected for the unscaled B3LYP ZPEs. All calculations using the 6–311+G* basis set. All energies in kcal/mol. The structures are sorted following the CCSD(T)//B3LYP stabilities, and identified according to the closest point group symmetry (see Figs. 2, 3, 4, 5, 6, 7). Strictly speaking, all structures belong to the C_1 group, as they are randomly produced during the annealing and then optimized without imposition of symmetry constraints. Isomer contributions estimated via standard Boltzmann population analyisis

Cluster	B3LYP			CCSD(T)//B3LYP		
	ΔE	BE/atom	pop (≈%)	ΔE	BE/atom	pop (≈%)
Li_5^q clusters						
Li_5^+, D_{3h}	0.00	21.85	97.43	0.00	21.63	99.40
Li_5^+, D_{2d}	2.15	21.42	2.57	3.03	21.02	0.60
$Li_5, C_{2v,a}$	0.00	14.84	95.24	0.00	15.21	93.79
Li_5, C_2	1.78	14.49	4.76	1.61	14.89	6.21
$Li_5^-, C_{2v,a}$	0.00	16.06	74.66	0.00	16.69	76.20
Li_5^-, C_{4v}	0.64	15.93	25.30	0.69	16.56	23.66
$Li_5^-, C_{2v,b}$	4.44	15.17	0.04	3.71	15.95	0.15
Li_6^q clusters						
$Li_6^+, C_{2v,a}$	0.00	22.29	100.00	0.00	22.02	100.00
$Li_6^+, C_{2v,b}$	10.76	20.50	≈ 0	12.73	19.90	≈ 0
Li_6^+, D_{2d}	12.95	20.14	≈0	13.72	19.74	≈ 0
Li_6, D_{4h}	0.00	17.02	99.44	0.00	17.68	99.67
Li_6, C_{5v}	3.10	16.51	0.53	3.44	17.10	0.30
Li_6, D_{3h}	4.79	16.23	0.03	4.77	16.88	0.03
Li_6^-, D_{4h}	0.00	18.09	100.00	0.00	18.85	100.00
Li_6^-, D_{3h}	6.89	16.95	≈0	9.54	17.26	≈ 0
$Li_6^-, C_{s,a}$	11.65	16.15	≈0	13.74	16.56	≈ 0
$Li_6^-, C_{s,b}$	17.61	15.16	≈0	19.53	15.59	≈ 0
$Li_6^-, D_{\infty h}$	19.42	14.86	≈0	21.78	15.22	≈ 0
Li_7^q clusters						
Li_7^+, D_{5h}	0.00	23.87	99.99	0.00	23.79	99.98
$Li_7^+, C_{3v,a}$	5.57	23.07	0.01	4.96	23.08	0.02
Li_7, D_{5h}	0.00	18.40	98.74	0.00	19.12	98.36
$Li_7, C_{3v,a}$	2.58	18.03	1.26	2.43	18.78	1.64
Li_7^-, D_{5h}	0.00	19.17	59.18	0.00	20.44	72.89
$Li_7^-, C_{3v,b}$	0.42	19.11	29.36	0.62	20.36	25.50
$Li_7^-, C_{3v,a}$	0.97	19.03	11.46	2.26	20.12	1.61
Li_7^-, C_s	12.67	17.36	≈ 0	16.10	18.14	≈0

QTAIM: $3D_{QT}$, $2D_{QT}$ or $1D_{QT}$. This will be useful to quantify any transitions or tendencies for clusters to change dimensionality. In order to address the issue of covalency in bonding within lithium clusters, we use the local total energy density at the BCP suggested earlier [57]:

$$\mathscr{H}(\mathbf{r}_b) = \mathscr{V}(\mathbf{r}_b) + \mathscr{G}(\mathbf{r}_b) \quad (2)$$

where a degree in covalent character is indicated by $\mathscr{H}(\mathbf{r}_b)<0$. Previously, one of us used Eq. 2 to explain the unusual strength in hydrogen bonds in ice I_h [58] in agreement with experiment [59]. All QTAIM properties were calculated using the AIMQB program within the AIMStudio suite, [60] using the Proaim basin integration method. For the lithium clusters where the electron density distributions are rather diffuse, the atomic integration radius was increased to 20 Å to get sufficient accuracy. The Promega (1st–Order) atomic basin integration method was used, again for the reasons of the diffuse nature of the electron density distributions.

Table 2 Energetic analysis for the $Li_{8,9}^{0,\pm1}$ clusters. See caption in Table 1 for additional description. Structures marked with asterisks come in enantiomer pairs, and therefore the calculated populations are twice what is predicted for each one

Cluster	B3LYP			CCSD(T)//B3LYP		
	ΔE	BE/atom	pop (≈ %)	ΔE	BE/atom	pop (≈ %)
Li_8^qclusters						
$Li_8^+C_{s,a}$	0.00	23.26	99.68	0.00	23.34	99.72
$Li_8^+C_{s,b}$	3.40	22.84	0.32	3.47	22.90	0.28
Li_8, T_d	0.00	19.08	62.70	0.00	20.07	55.33
Li_8,C_{3v}	0.71	18.99	18.83	0.33	20.03	31.52
Li_8,$C_{s,a}$	0.72	18.99	18.47	0.85	19.97	13.15
Li_8^-, D_{2d}	0.00	19.71	89.20	0.00	20.89	96.90
Li_8^-, $C_{s,a}$	1.36	19.54	9.06	2.13	20.62	2.68
Li_8^-, $C_{2v,a}$	2.41	19.41	1.53	3.22	20.49	0.42
Li_8^-, $C_{s,c}$	9.51	18.52	≈0	12.40	19.34	≈0
Li_8^-, $C_{2v,b}$	3.71	19.24	0.17	19.05	18.51	≈0
Li_8^-, D_{2h}	16.47	17.65	≈0	20.23	18.36	≈0
Li_8^-, $C_{s,d}$	15.87	17.72	≈0	20.44	18.33	≈0
Li_8^-, C_1	16.42	17.66	≈0	20.85	18.28	≈0
Li_8^-, $C_{2v,c}$	21.83	16.98	≈0	27.29	17.48	≈0
Li_8^-, C_{2h}	4.54	19.14	0.04	28.59	17.31	≈0
Li_8^-, $C_{s,e}$	18.19	17.43	≈0	36.16	16.37	≈0
Li_9^qclusters						
Li_9^+, D_{4d}	0.00	24.37	99.98	0.00	24.85	100.00
Li_9^+, $C_{2v,a}$	5.10	23.80	0.02	6.30	24.15	≈0
Li_9^+, $C_{3v,a}$	9.59	23.30	≈0	11.05	23.62	≈0
Li_9^+, $C_{s,a}$	16.93	22.49	≈0	19.72	22.66	≈0
Li_9^+, $C_{2,a}^*$	18.40	22.33	≈0	20.35	22.59	≈0
Li_9^+, $C_{s,b}$	22.06	21.92	≈0	24.99	22.07	≈0
Li_9,$C_{2v,b}$	0.26	19.11	36.92	0.00	20.01	87.50
Li_9,$C_{2v,a}$	1.38	18.99	5.56	1.16	19.88	12.38
Li_9,$C_{s,a}$	3.55	18.75	0.14	4.22	19.54	0.07
Li_9,C_{4v}	0.00	19.14	57.36	4.57	19.50	0.04
Li_9,$C_{3v,a}$	5.17	18.57	0.01	5.13	19.44	0.02
Li_9^-, $C_{s,c}$	0.00	20.19	59.12	0.00	21.43	71.33
Li_9^-, $C_{2,a}^*$	1.04	20.07	20.20	1.10	21.31	22.15
Li_9^-, $C_{s,a}$	0.62	20.12	20.59	1.42	21.27	6.49
Li_9^-, $C_{2v,a}$	3.83	19.76	0.09	4.70	20.91	0.03
Li_9^-, $C_{2,b}$	5.36	19.59	0.01	6.18	20.75	≈0
Li_9^-, $C_{3v,a}$	6.49	19.47	≈0	7.45	20.60	≈0
Li_9^-, $C_{3v,b}$	7.47	19.36	≈0	9.03	20.43	≈0
Li_9^-, $C_{2v,c}$	10.86	18.98	≈0	9.46	20.38	≈0
Li_9^-, $C_{s,d}$	16.43	18.36	≈0	20.40	19.16	≈0
Li_9^-, $C_{2v,d}$	17.84	18.20	≈0	21.67	19.02	≈0

Table 3 Energetic analysis for the $Li_{10}^{0,\pm1}$ clusters. See caption in Table 1 for additional description. Structures marked with asterisks come in enantiomer pairs, and therefore the calculated populations are twice what is predicted for each one

Cluster	B3LYP			B3LYP		
	ΔE	BE/atom	pop (≈%)	ΔE	BE/atom	pop (≈%)
Li_{10}^qclusters						
Li_{10}^+,C_{4v}	0.00	23.66	98.72	0.00	24.10	99.71
Li_{10}^+,$C_{s,a}$	3.48	23.31	0.28	3.84	23.72	0.15
Li_{10}^+, D_{2d}	2.76	23.38	0.93	4.09	23.69	0.10
Li_{10}^+, $C_{s,b}$	4.30	23.23	0.07	4.66	23.63	0.04
Li_{10}, D_{2d}	0.00	19.88	95.98	0.00	20.85	64.36
Li_{10},$C_{s,a}$	2.08	19.67	2.87	0.55	20.80	25.58
Li_{10}, $C_{1,a}^*$	3.03	19.58	1.15	1.51	20.70	5.03
Li_{10},$C_{s,c}$	7.52	19.13	≈0	7.10	20.14	≈0
Li_{10}^-, $C_{s,d}$	0.13	20.34	17.81	0.00	21.53	34.90
Li_{10}^-, C_2^*	0.00	20.36	44.06	0.29	21.51	42.98
Li_{10}^-, $C_{1,a}^*$	0.49	20.31	19.16	0.72	21.46	20.84
Li_{10}^-, $C_{1,b}$	2.34	20.12	0.42	2.45	21.29	0.56
Li_{10}^-, $C_{s,e}$	2.18	20.14	0.55	2.57	21.28	0.46
Li_{10}^-, $C_{s,f}$	2.91	20.06	0.16	3.18	21.22	0.16
Li_{10}^-, $C_{1,c}$	3.16	20.04	0.11	3.75	21.16	0.06
Li_{10}^-, $C_{1,d}$	4.23	19.93	0.02	4.54	21.08	0.02
Li_{10}^-, $C_{1,e}^*$	3.95	19.96	0.03	4.86	21.05	0.02
Li_{10}^-, $C_{s,g}$	5.24	19.83	≈0	5.98	20.94	≈0
Li_{10}^-, $D_{2h,a}$	0.13	20.34	17.64	6.12	20.92	≈0
Li_{10}^-, $C_{s,c}$	4.52	19.90	0.01	6.18	20.92	≈0
Li_{10}^-, $C_{s,h}$	8.48	19.51	≈0	10.09	20.53	≈0
Li_{10}^-, $C_{s,i}$	9.46	19.41	≈0	11.07	20.43	≈0
Li_{10}^-, $D_{2h,b}$	20.12	18.34	≈0	28.53	18.68	≈0
Li_{10}^-, $C_{s,j}$	26.79	17.68	≈0	33.22	18.21	≈0
Li_{10}^-, C_{2h}	31.15	17.24	≈0	38.77	17.66	≈0

Results and discussion

ASCEC conditions

We used two distinct approaches to construct the initial geometries for Li_n^q ASCEC runs: superimposing all atoms at the center of a cubic box in a big bang–like fashion, or placing them as far apart from each other as possible within the boundaries of the cubic box; whatever the choice, each collection of atoms was allowed to evolve as overall cationic, neutral or anionic systems under the annealing conditions. The annealing was run at least twice for each PES. The systems were placed inside cubes of varying lengths depending on the number of atoms in the cluster. The HF/lanl2dz model chemistry was used to calculate the energy of Markovian chains of randomly generated cluster configurations; we used geometrical quenching routes with initial temperatures of 500 K, a constant temperature decrease of 5% and 100 total temperatures.

Geometries and structural issues

The number of local extrema in a given PES increases exponentially with the number of atoms, [49] therefore, the amount of theoretical or experimental work needed for complete characterization of PESs of the complexities of our subjects is prohibitively large, rendering that aspiration impractical.

In this work, 18 conformational spaces of Li clusters were explored, Li_n^q (n=5−10, q=0, ±1), out of which nine are closed shell and nine are open shell systems. Despite not having chiral centers, a number of optical isomers were found due to the overall spatial arrangement of the atoms. A total of 94 stable structures within 68 geometrical motifs were located by our methodology; the structures are distributed into 40 closed shell and 54 open shell clusters. There are a total of 20 cationic, 20 neutral and 54 anionic clusters, as shown in Fig. 1; it can be seen that anionic clusters have richer conformational spaces with 2:1 (and larger) ratios in the number of structures when compared to neutral and to cationic clusters of similar sizes; large numbers of anionic open shell systems lead to comparatively more complex conformational spaces for anionic clusters (Fig. 1); on the other hand, the ratios between the number of neutral and cationic clusters remains quite similar (≈ 1:1) regardless of number of electrons in the outermost shell.

The geometrical motifs for each size are depicted in Figs. 2, 3, 4, 5, 6, 7. Tables 1, 2, 3 list along with relevant energy results, the closest point group for all equilibrium geometries. The following observations are drawn after analyzing the structures and energies encountered in this work: (*i*) Neutral and charged microclusters of the same size have very different conformational possibilities except for Li_7. (*ii*) CCSD(T) and B3LYP energies predict that n=5 is the transition point from planar to 3D (Euclidean) structural preferences in all cations (for Li_5^+, the most stable structure is 3D); Li_6, Li_6^- prefer 3D structures. (*iii*) There are four types of structures, which according to euclidean geometry we label 1D, 2D, *semi*−2D and *open*−3D, that only exist for anionic clusters and therefore contribute to the structural diversity of these charged systems: $D_{\infty h}$(n=6) is 1D. $C_{2v,b}$(n=5); $C_{s,a}$,$C_{s,b}$(n=6); C_s (n=7); D_{2h},$C_{2v,c}$,$C_{s,e}$(n=8); $C_{2v,d}$ (n=9) and $D_{2h,b}$,$C_{s,\ j}$, C_{2h}(n=10) are 2D. $C_{s,d}$,C_1(n=8) and $C_{s,d}$ (n=9) are *Semi*−2D. $C_{s,c}$ (n=8); $C_{3v,b}$(n=9) and $C_{s,h}$,$C_{s,i}$(n=10) are *open*−3D. Comparatively small HOMO energies and binding energies for these systems suggest that the excess electron is weakly bound in this set of anionic clusters.

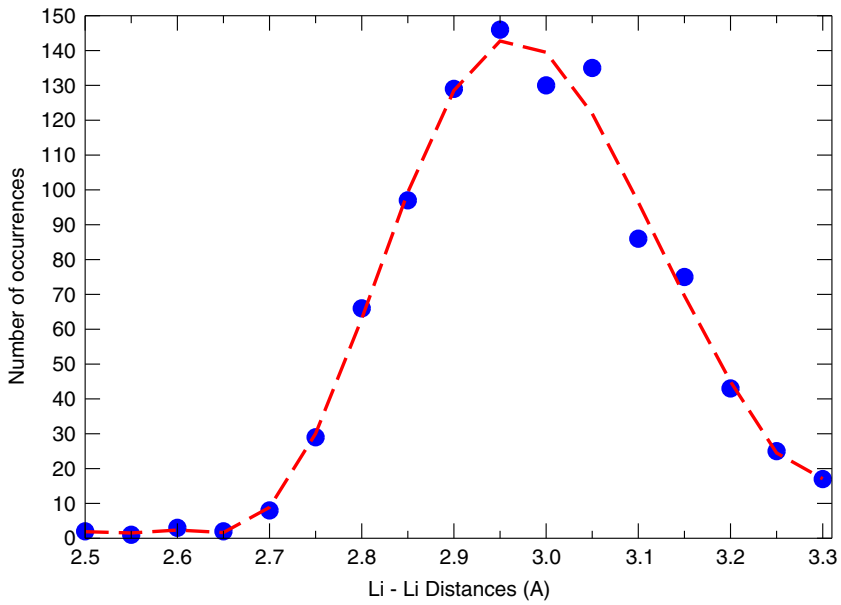

Fig. 8 Distribution of the Li···Li distances (Å, first neighbors) in the anionic Lin, n=5−10 clusters. An approximate gaussian distribution centered around≈ 2.95 Å is predicted. Similar trends with fewer occurrences are calculated for neutral and cationic clusters

Table 4 Statistically weighted properties for the Li_n^q clusters. All quantities in kcal/mol. IPs are for the neutral clusters

n	Cations			Anions			Neutrals			
	BE/atom			BE/atom			BE/atom		IP	
	B3LYP	CCSD (T)	Exp[4]	B3LYP	CCSD (T)	B3LYP	CCSD (T)	Exp[4]	CCSD (T)	Exp[1]
5	22.42	22.20	24.21	16.49	17.13	15.33	15.69	17.89	3.96	4.02
6	22.90	22.63	24.79	18.68	19.44	17.64	18.30	20.22	4.25	4.20
7	24.54	24.46	25.66	19.78	21.05	19.04	19.79	20.89	3.95	3.94
8	23.92	24.00	25.42	20.33	21.52	19.73	20.72	21.88	4.23	4.16
9	25.08	25.56	26.70	20.80	22.06	19.81	20.68	21.32	3.47	3.29
10	24.33	24.79	25.94	21.15	22.18	20.60	21.55	22.62	3.97	3.95

Approximate gaussian radial distributions are predicted for Li· · ·Li distances for all clusters considered in this study. Figure 8 plots the Li· · ·Li distances for all anionic clusters, similar trends with fewer occurrences are calculated for neutral and cationic clusters. Li· · ·Li distances for the same geometrical motif but different charges decrease as $r_{cation} > r_{anion} > r_{neutral}$. In other words, neutrals are more compact than anions and these than cations for the same structural pattern in the same number of atoms. For larger clusters, addition of individual atoms seem to energetically favor structures where new fused tetrahedra are formed; this observation has previously been noticed by Boustani and coworkers [12]. A closer look at the most stable structures of the larger clusters reveals that several of them have the D_{5h} structure for seven atoms (Fig. 4) as basic unit, in some cases, complex geometrical fusions of the same structure lead to very stable clusters.

Energies, cluster stabilization and other properties

In 1994, Bréchignac et al. [4] presented atomization energies of cationic lithium clusters derived from rates of unimolecular decay in an evaporative ensemble. The same study also included cohesive energies of the corresponding neutral clusters, derived from the cationic values using the experimental ionization potentials measured by Dugourd and coworkers [1]. The most relevant calculated energetic information for all clusters considered in this study are listed in Tables 1, 2, 3.

As a general rule, for larger sizes, compact structures are energetically preferred over open or planar conformations. One interesting observation is that for all neutral and anionic clusters, local minima appear very close in energy to the global minimum, leading to contributions from several sources to the overall stability of those systems. On the other hand, cationic clusters always show dominant contributions from one particular structure (Tables 1, 2, 3). Notice that the statistically weighted binding energies per atom increase monotonically as a function of the cluster size for anionic clusters while local fluctuations are observed for both neutral and cationic systems (Table 4, Fig. 9). We point out that the CCSD(T)//B3LYP calculated binding energies/atom reproduce very well the available experimental data (Table 4, Fig. 9); there is also a remarkable agreement (with few exceptions) between B3LYP and CCSD(T)//B3LYP binding energies values with deviations of≈0.27, 0.76 and 1.03 kcal/mol in average for cations, neutrals and anions, respectively. For the calculated BE/atom, it should also be noticed that the singly charged clusters are more stable than the neutral ones, with the

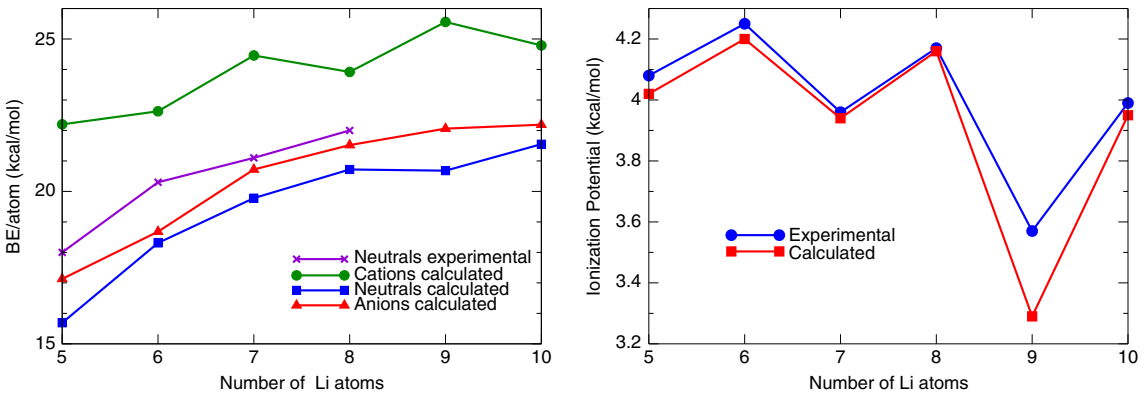

Fig. 9 CCSD(T)//B3LYP Binding energies per atom for neutral and charged Li microclusters (left). Experimental data taken from Bréchignac et al. [4] Ionization potential for neutral Li microclusters (right). Experimental data taken from [1]

cationic clusters being the most stable. Ionization potential is a valuable electronic property involved in the reactivity of a molecular system. Figure 9 shows the statistically weighted IPs computed at the B3LYP/6–311+G(d) level as a function of the cluster size; an oscillatory behavior is observed due to alternations between open and closed shells, for odd and even number of electrons respectively. A remarkable coincidence is also observed between our calculated statistically weighted IPs and the experimental data for neutral clusters by about 0.08 eV in average. This satisfactory agreement is an indication of the good quality of the geometries produced by the stochastic exploration of the conformational spaces for the title clusters. We offer next a discussion of cluster stability in terms of the topological properties of the electron densities.

Topological analysis of the electron densities

Tables 5, 6, 7 list all relevant quantities for the topological analysis of the electron charge distributions for Li_n^q clusters.

Table 5 Topological analysis of the electron charge distributions for $Li_{5,6,7}^{0,\pm1}$ clusters: critical point data for the four sets of critical points, NNAs, BCPs, RCPs and CCPs, see the main text for further explanation. The number of lithium atoms equals the number of NCPs in every case. The sum of the NNAs, BCPs, RCPs and CCPs is given by $\sum_{ABRC}$. The quantum topological dimension of each cluster is given by DQT; [39] "structural motifs" refers to the structural subunits described in Fig. 11. The structures are sorted following the CCSD(T)//B3LYP stabilities, and identified according to the closest point group symmetry

Cluster	NNA	BCP	RCP	CCP	$\sum_{ABRC}$	D_{QT}	Structural motifs
Li_5^qclusters							
Li_5^+, D_{3h}	2	9	3	0	14	2	A_1
Li_5^+, D_{2d}	2	6	0	0	8	1	$B_{1p,C}$
Li_5,$C_{2v,a}$	3	8	1	0	12	2	B_1
Li_5,C_2	2	8	2	0	12	2	B_1
$Li_5^-, C_{2v,a}$	3	9	2	0	14	2	C
Li_5^-, C_{4v}	4	12	4	0	20	2	B_1
$Li_5^-, C_{2v,b}$	2	6	0	0	8	1	B_{1p}
Li_6^q clusters							
$Li_6^+, C_{2v,a}$	2	9	2	0	13	2	D
$Li_6^+, C_{2v,b}$	2	7	0	0	9	1	B_{1p}, C
Li_6^+, D_{2d}	3	8	0	0	11	1	B_{1p}, C
Li_6, D_{4h}	4	16	9	2	31	3	A_1, C
Li_6,C_{5v}	10	25	10	0	45	2	A_1, C
Li_6, D_{3h}	3	9	1	0	13	2	B_1, B_{1p}
Li_6^-, D_{4h}	4	16	9	2	31	3	A_1, C
Li_6^-, D_{3h}	3	11	3	0	17	2	B_1, B_{1p}
$Li_6^-, C_{s,a}$	3	10	2	0	15	2	B_{1p}
$Li_6^-, C_{s,b}$	4	9	0	0	13	1	B_{1p}
$Li_6^-, D_{\infty h}$	5	10	0	0	15	1	B_{1p}
Li_7^q clusters							
Li_7^+, D_{5h}	5	20	11	2	38	3	A_1, C
$Li_7^+, C_{3v,a}$	3	15	6	0	24	2	D
Li_7, D_{5h}	10	23	9	2	44	3	A_1, C
Li_7,$C_{3v,a}$	3	12	4	1	20	3	D
Li_7^-, D_{5h}	5	17	7	1	30	3	A_1, C
$Li_7^-, C_{3v,b}$	6	18	7	1	32	3	C
$Li_7^-, C_{3v,a}$	4	12	3	1	20	3	D
Li_7^-, C_s	4	13	3	0	20	2	A_1, B_{1p}

Table 6 Topological analysis of the electron charge distributions for $Li_{8,9}^{0,\pm1}$ clusters. See caption in Table 5 for additional description. Structures marked with asterisks come in enantiomer pairs

Cluster	NNA	BCP	RCP	CCP	$\sum_{ABRC}$	D_{QT}	Structural motifs
Li_8^qclusters							
$Li_8^+, C_{s,a}$	4	14	4	1	23	3	D
$Li_8^+, C_{s,b}$	3	16	6	0	25	2	D
Li_8, T_d	4	22	12	1	39	3	D
Li_8,C_{3v}	4	14	4	1	23	3	D
Li_8,$C_{s,a}$	4	17	7	1	29	3	D
Li_8^-, D_{2d}	4	14	4	1	23	3	C,D
$Li_8^-, C_{s,a}$	3	14	5	1	23	3	D
$Li_8^-, C_{2v,a}$	4	18	9	2	33	3	D
$Li_8^-, C_{s,c}$	2	14	5	0	21	2	$B_{1p,}$ D
$Li_8^-, C_{2v,b}$	4	14	3	0	21	2	B_{1p}
Li_8^-, D_{2h}	4	12	1	0	17	2	$A_{1p,}$ B_{1p}
$Li_8^-, C_{s,d}$	5	17	5	0	27	2	$B_{1p,}$ B_{1p}
Li_8^-, C_1	4	14	3	0	21	2	$B_{1p,}$ B_{1p}
$Li_8^-, C_{2v,c}$	4	12	1	0	17	2	$B_{1p,}$ B_{1p}
Li_8^-, C_{2h}	5	14	2	0	21	2	$B_{1p,}$ B_{1p}
$Li_8^-, C_{s,e}$	5	13	1	0	19	2	$B_{1p,}$ B_{1p}
Li_9^q clusters							
Li_9^+, D_{4d}	8	24	8	0	40	2	C,D
$Li_9^+, C_{2v,a}$	5	20	8	1	34	3	D
$Li_9^+, C_{3v,a}$	4	15	3	0	22	2	D
$Li_9^+, C_{s,a}$	6	17	4	1	28	3	D
$Li_9^+, C_{2,a}^*$	4	18	6	0	28	2	D
$Li_9^+, C_{s,b}$	4	19	7	0	30	2	D
Li_9,$C_{2v,b}$	4	20	8	0	32	2	C,D
Li_9,$C_{2v,a}$	4	19	11	4	38	3	C,D
Li_9,$C_{s,a}$	4	22	12	2	40	3	D
Li_9,C_{4v}	4	17	7	2	30	3	D
Li_9,$C_{3v,a}$	5	21	9	1	36	3	$A_{1p,}$ D
$Li_9^-, C_{s,c}$	4	16	6	2	28	3	D
$Li_9^-, C_{2,a}^*$	5	18	5	0	28	2	D
$Li_9^-, C_{2v,a}$	4	16	5	1	26	3	D
$Li_9^-, C_{2,b}$	4	15	3	0	22	2	D
$Li_9^-, C_{3v,a}$	3	11	0	0	14	1	A_{1p}
$Li_9^-, C_{3v,b}$	5	13	0	0	18	1	A_{1p}
$Li_9^-, C_{2v,c}$	5	15	3	1	24	3	A_{1p},D
$Li_9^-, C_{s,d}$	8	19	3	0	30	2	$B_{1,}$ B_{1p}
$Li_9^-, C_{2v,d}$	5	16	3	0	24	2	$B_{1,}$ B_{1p}

Table 7 Topological analysis of the electron charge distributions for $Li_{10}^{0,\pm1}$ clusters. See caption in Table 5 for additional description. Structures marked with asterisks come in enantiomer pairs. Structure Li_{10}^{-}, $C_{s,h}$ does not satisfy Eq. 1

Cluster	NNA	BCP	RCP	CCP	$\sum_{ABRC}$	D_{QT}	Structural motifs
Li_{10}^{q}clusters							
Li_{10}^{+}, C_{4v}	4	25	12	0	41	2	*C,D*
$Li_{10}^{+}, C_{s,a}$	6	20	5	0	31	2	*D*
Li_{10}^{+}, D_{2d}	6	26	15	4	51	3	*C,D*
$Li_{10}^{+}, C_{s,b}$	5	22	9	1	37	3	*D*
Li_{10}, D_{2d}	6	22	11	4	43	3	*C,D*
Li_{10},$C_{s,a}$	5	19	5	0	29	2	*D*
Li_{10}, $C_{1,a}^{*}$	5	21	9	2	37	3	*D*
Li_{10},$C_{s,c}$	5	23	10	1	39	3	*D*
$Li_{10}^{-}, C_{s,d}$	8	22	6	1	37	3	*D*
Li_{10}^{-}, C_{2}^{*}	6	20	7	2	35	3	*D*
$Li_{10}^{-}, C_{1,a}^{*}$	5	18	4	0	27	2	*D*
$Li_{10}^{-}, C_{1,b}$	5	21	9	2	37	3	*D*
$Li_{10}^{-}, C_{s,e}$	6	22	9	2	39	3	*D*
$Li_{10}^{-}, C_{s,f}$	4	20	8	1	33	3	*D*
$Li_{10}^{-}, C_{1,c}$	5	24	11	1	41	3	*D*
$Li_{10}^{-}, C_{1,d}$	5	17	3	0	25	2	*D*
$Li_{10}^{-}, C_{1,e}^{*}$	4	20	8	1	33	3	*D*
$Li_{10}^{-}, C_{s,g}$	3	12	0	0	15	1	B_{1p}
$Li_{10}^{-}, D_{2h,a}$	4	20	11	4	39	3	*D*
$Li_{10}^{-}, C_{s,c}$	4	19	8	2	33	3	*D*
$Li_{10}^{-}, C_{s,i}$	5	19	6	1	31	3	B_{1p}
$Li_{10}^{-}, D_{2h,b}$	4	16	3	0	23	2	B_{1p}, B_{1p}
$Li_{10}^{-}, C_{s,j}$	6	18	3	0	27	2	B_{1p}, B_{1p}
Li_{10}^{-}, C_{2h}	6	20	5	0	31	2	B_{1p}, B_{1p}

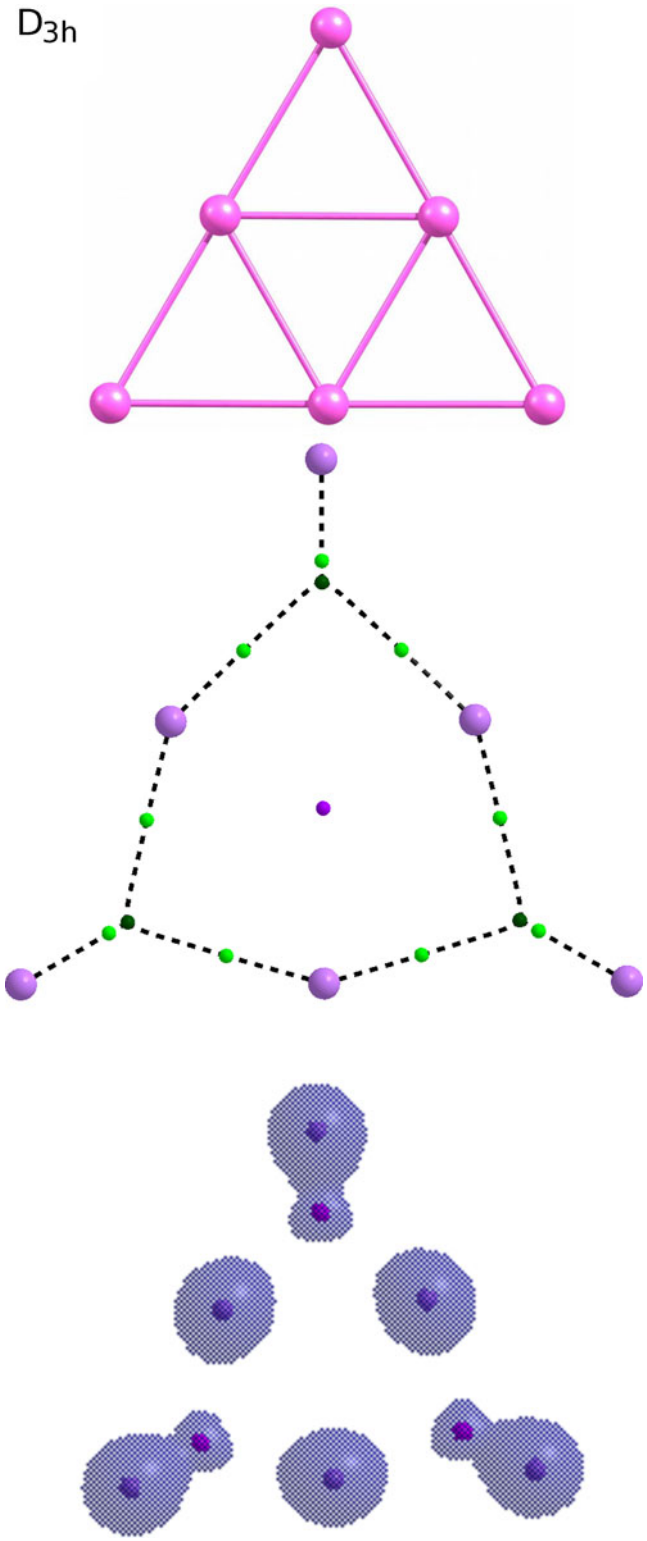

Fig. 10 Geometry, critical points and electron density for the *D3h* cluster in neutral Li_6. NNAs are responsible for overall stability of the clusters. The pseudoatoms are surrounded by regions of high electron density. Lines joining atoms (top) are drawn to help visualize the geometrical motif

The first striking feature about bonding in the clusters in this study, already pointed out by other works [19–21, 61, 62], is that there are no directly bonded pairs of Li atoms among the most stable structures, this holds regardless of charge, size or geometry. Instead, bonding seems to occur via non–nuclear attractors (NNAs), positioned between Li atoms: well defined bond critical points (BCPs) are located in the lines joining Li – NNA pairs, as seen for one illustrative case in Fig. 10. NNAs, also known as "pseudoatoms", which are regions of local maximum electron density not surrounding a nucleus, have been controversially invoked in the past to help explain among other things metal–metal bonding. A very recent report by Platts and coworkers, [63] offers for the first time, experimental characterization of a theoretically predicted NNA; in that particular study, a NNA is found to stabilize a Mg – Mg bond in a stable molecule. For Li_2, Glaser et al. [64] suggested that the NNA arises from a symmetric combination of valence 2*s* orbitals with smaller contributions from 2 p_z orbitals. It has been argued that the stability of long bonds with low polarities, negligible contributions from core orbitals, and major radial contributions from the valence orbitals to the

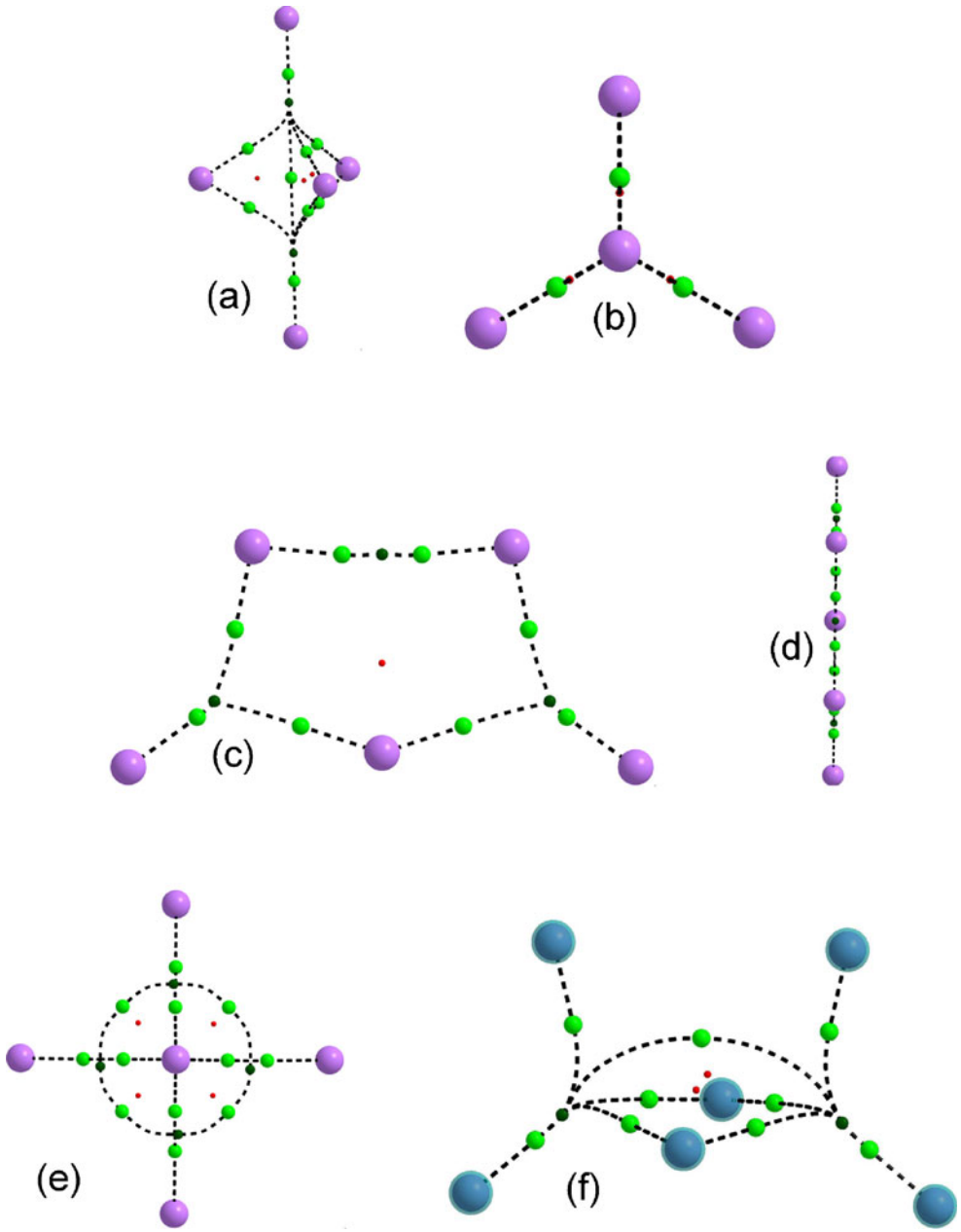

Fig. 11 Basic structural motifs in this work. In sub–figures (**a**) and (**b**) two basic motifs are shown, where (**b**) is an orthogonal projection of (**a**), these are referred to in this work as basic structural motifs A_1 and its 2D projection $A_{1\ p}$ respectively. Sub–figures (**c**) and (**d**) show two additional structural motifs, where (**d**) is an orthogonal projection of (**c**) in the plane of (**c**); these structural motifs are referred to as basic structural motifs B_1 and its 2D projection $B_{1\ p}$ respectively. Sub–figures (**e**) and (**f**) show the basic structural motifs C and D

electron densities would benefit considerably from the presence of NNAs intermediate between the atoms [64, 65]. Electron configuration of lithium atoms satisfy the above requirements, in addition, the predicted long Li· · ·Li

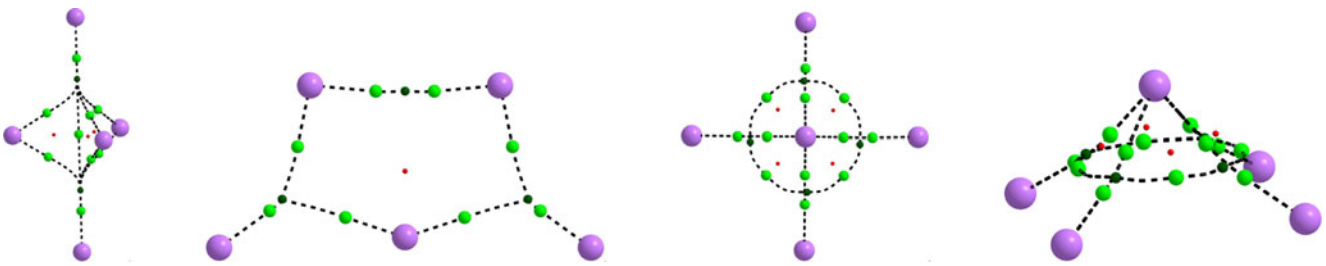

Fig. 12 The critical point sets. NCPs, NNAs, BCPs and RCPs, of the topologies of the charge density for the most energetically stable lithium clusters containing five lithium nuclei for the three cluster types with respect to their charge. Traveling from left to right the cationic, neutral and two views of the anionic clusters are shown

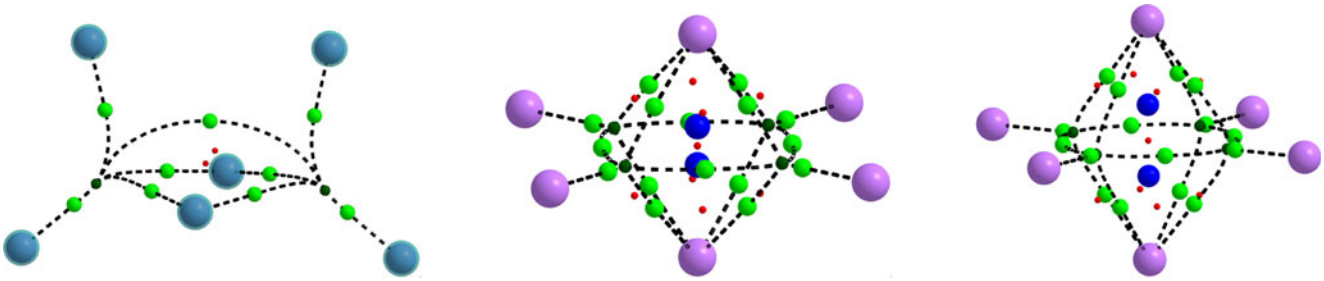

Fig. 13 The critical point sets. NCPs, NNAs, BCPs and RCPs, of the topologies of the charge density for the most energetically stable lithium clusters containing six lithium nuclei for the three cluster types with respect to their charge. Traveling from left to right the cationic, neutral and anionic clusters are shown. In the cationic cluster all six of the lithium nuclei are highlighted (seen in larger blue spheres in the electronic version), this is because this structure is basic structural motif *D*, which is present in larger more structurally complex structures, see Figs. 15, 16, 17, where the structural motif is highlighted

distances reported here for Li clusters (Fig. 8) probably arise from the stabilizing presence of NNAs. There is no correlation between the number of bond, ring or cage critical points with relative stability of the clusters (Tables 5, 6, 7).

Creation of structural motifs and cluster growth

The limitations of both quantum topology and the use of point group symmetries are that they alone can not decompose an individual cluster in order to provide some hints to mechanisms of cluster growth. In order to probe the structural changes with cluster growth we will use two main approaches. First, we create structural motifs based on 2D projections, examples of such 2D projections can be seen in Fig. 11, where (b) is a 2D projection of (a) and (d) is a 2D projection of (c). A variation of this 2D projection approach is to allow 'dynamic' motifs that include more intricate versions, an example of this is Fig. 11 (e), where this dynamic motif has four lithium nuclei radially positioned; this motif appears unchanged in Fig. 12 (anion) and in Fig. 13 (neutral, anion); a variation of the theme with five radially positioned lithium nuclei appears in Fig. 14 (cation, neutral, anion); variations are also observed for Fig. 15 (anion) and with eight radially positioned lithium atoms for the cationic and neutral clusters of nine (Fig. 16) and ten lithium atoms (Fig. 17). The second approach to structural decomposition is simply to choose a group of nuclei as the basic motif and search for the same group with approximately similar internal coordinates to each other in larger clusters. The basic structural pattern for this type of motif is given in Fig. 11 (f). Figure 13 (neutral), Fig. 15 (neutral, cationic, anionic), contain this motif as do the neutral and cationic clusters of nine (Fig. 16) and ten (Fig. 17) lithium atoms.

In order to understand why the 2D projections may be useful for the decomposition of clusters, the reader is asked to first imagine a regular cylinder with its long axis parallel to the *z*–axis and the circular cross section in the *xy* plane. Then we wish to decompose this 3D object into the fewest 2D objects that best capture the character of the cylinder. Then perhaps, by imaging a 2D universe it is possible to decompose such a 3D object by passing a pair of bisecting perpendicular planes through the cylinder to create the orthogonal structural sub–units of a rectangle and a circle.

We use this method of 2D projections in partnership with structural motifs to follow changes in cluster topology with growth. The choice of motifs can not be unique since our choice is abstract and therefore can not relate to actual growth processes, but it is a self referential characterization which we think yields more information than symmetry use alone. The use of symmetry only provides the generalized principle (not always holding) that more energetically stable structures tend to possess larger numbers of symmetry operations, which is less useful in situations where none of the

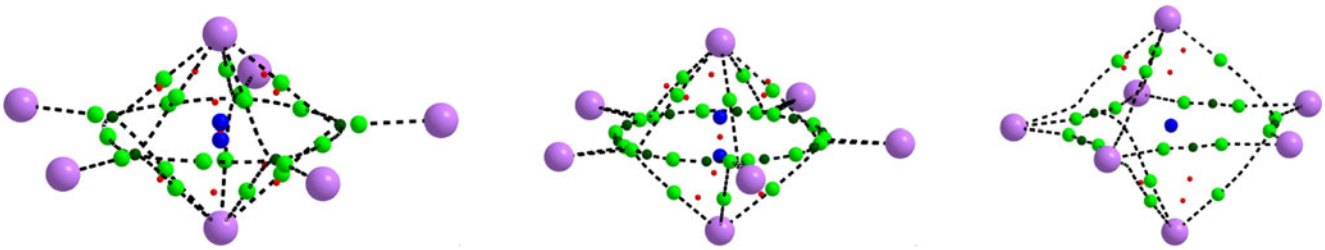

Fig. 14 The critical point sets. NCPs, NNAs, BCPs and RCPs, of the topologies of the charge density for the most energetically stable lithium clusters containing seven lithium nuclei for the three cluster types with respect to their charge. Traveling from left to right the cationic, neutral and anionic clusters are shown

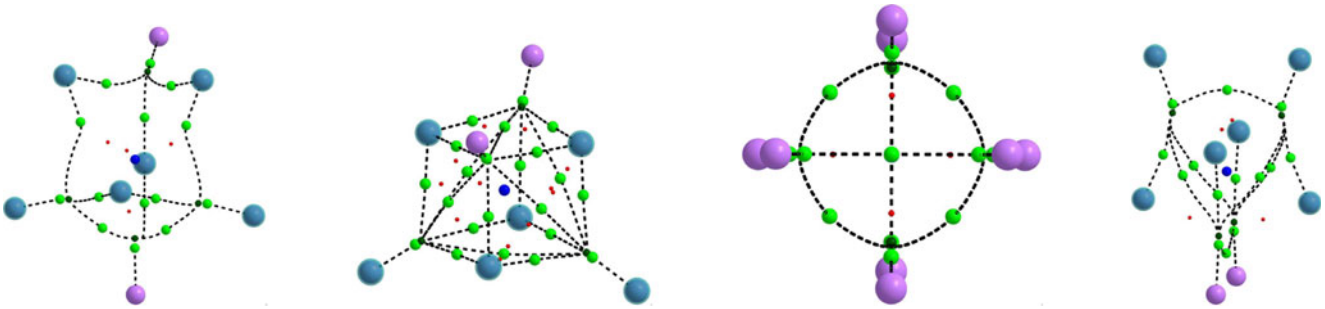

Fig. 15 The critical point sets. NCPs, NNAs, BCPs and RCPs, of the topologies of the charge density for the most energetically stable lithium clusters containing eight lithium nuclei for the three cluster types with respect to their charge. Traveling from left to right the cationic, neutral and two views of the anionic clusters are shown

structures under study have higher symmetries. An example of the limitations of reliance on symmetry operations is that of the case where the symmetry is lowered due to Jahn–Teller distortions because of degeneracy of partially occupied valence orbitals [66–69].

In Fig. 11 the basic structural motives that we will use to follow the growth of the lithium clusters, A_1, $A_{1\ p}$, B_1, $B_{1\ p}$, C and D are presented in sub–figures (a)–(f) respectively. In Figs. 12, 13, 14, 15, 16, 17 the critical point set for the most energetically stable lithium clusters of sizes five to ten respectively are presented for each of the charge types, cationic, neutral and anionic. The lithium nuclei that are highlighted in blue, in the electronic version of this work, are to show the embedded structural motif D for clarity in more complex structures. Tables 5, 6, 7 list the critical point data for the four sets of critical points for lithium clusters: NNA, BCP, RCP and CCP, including the dimensionality of each cluster within the quantum topology and the new structural motifs.

The results in this work allow us to venture descriptions of cluster growth. We start by using QTAIM to analyze the array of lithium clusters presented in Tables 5, 6, 7 for clusters of sizes five–ten respectively. Figures 12, 13, 14, 15, 16, 17 show the most energetically stable structures for

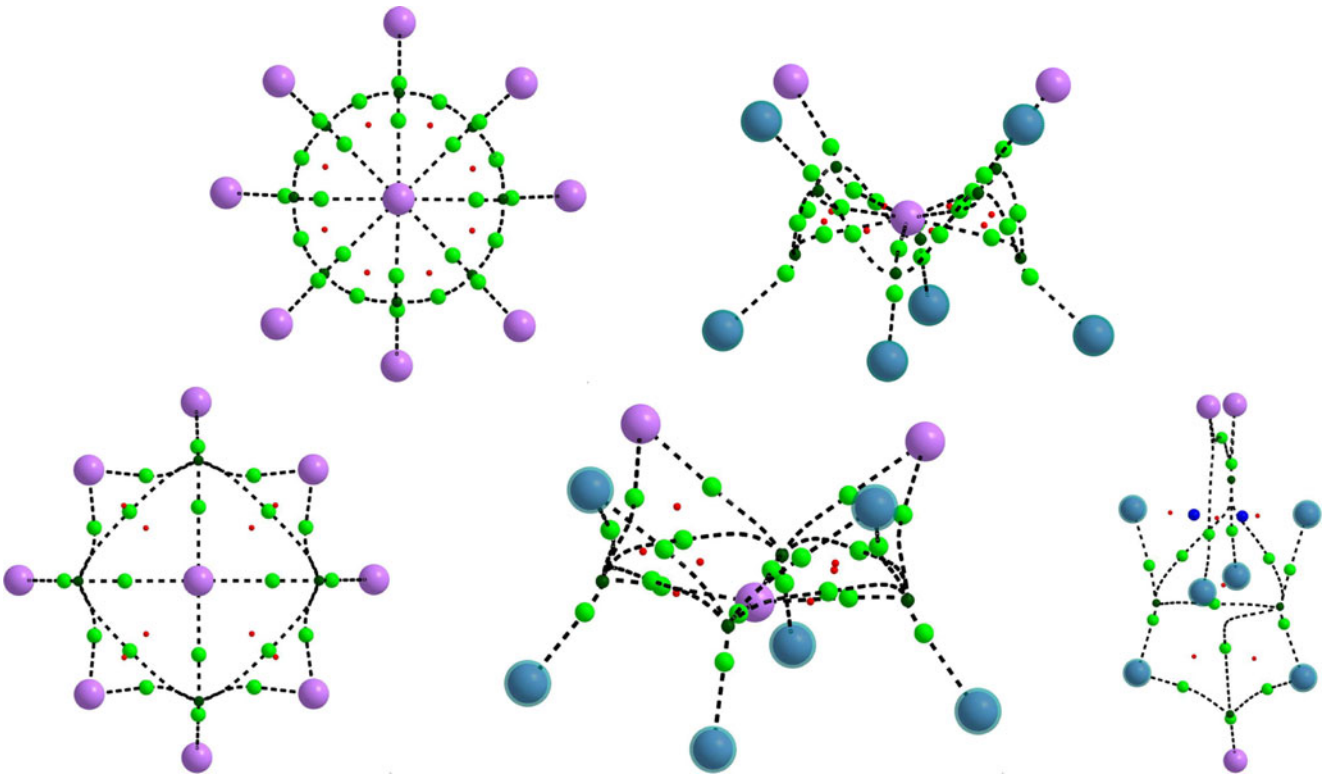

Fig. 16 The critical point sets. NCPs, NNAs, BCPs and RCPs, of the topologies of the charge density for the most energetically stable lithium clusters containing nine lithium nuclei for the three cluster types with respect to their charge. Traveling from left to right two views of the cationic (top), two views of the neutral (bottom) and one view of the anionic (bottom) clusters are shown

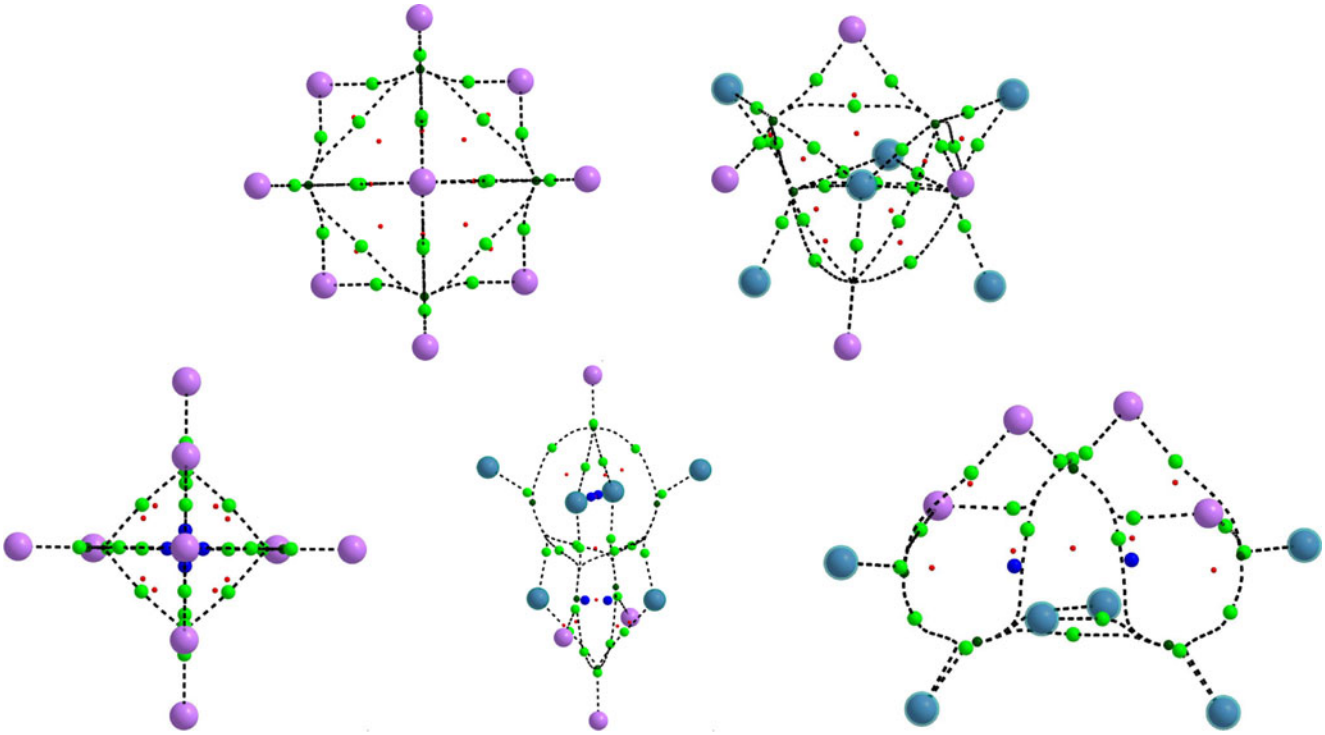

Fig. 17 The critical point sets. NCPs, NNAs, BCPs and RCPs, of the topologies of the charge density for the most energetically stable lithium clusters containing ten lithium nuclei for the three cluster types with respect to their charge. Traveling from left to right two views of the cationic (top), two views of the neutral (bottom) and one view of the anionic (bottom) clusters are shown

each charge type. Using QTAIM it can quickly be established that in the smallest clusters (Li_5, see Table 5 and Fig. 12), no CCPs are present in any structure, some structures do not have RCPs either and so are $1D_{QT}$, although this is not the case for the most stable; in other words, the most stable structures are $2D_{QT}$. For the Li_6 clusters (see Fig. 13), CCPs are now present in the most stable neutral and anionic structures, some of the less stable structures are $2D_{QT}$. This trend of increasing cluster quantum topology dimensions with energetic stability persists for larger sizes.

The topological complexity $\sum_{ABRC}$ steadily increases in Table 5, but there is a decrease in the symmetry and topological complexity in Table 6.

Examination of the structural motifs in Tables 5, 6, 7 shows more clearly the distinction between the most and least energetically stable structures than can be inferred from the quantum topology or the symmetry. The least stable structures being comprised more often of the projection motifs $A_{1\ p}$, $B_{1\ p}$ and the planar motif B_1. There is a clear boundary between clusters of size seven and eight in terms of the structural motifs present. We can clearly see from Tables 5, 6, 7 a transition between Li_{5-7} and Li_{8-10} in terms of the structural motifs; clusters $Li_{8,9,10}$ show a complete absence of motifs A_1, $A_{1\ p}$, B_1 and $B_{1\ p}$ (except for Li_9,$C_{3v,a}$ which contains $A_{1\ p}$), unlike clusters $Li^q_{5,6,7}$. The projection motif $B_{1\ p}$, is quantum topologically $1D_{QT}$ and its increasingly dominant presence, with increase in cluster size, amongst the least energetically stable structures shows that planar character correlates inversely with cluster size; this is especially true for the anionic clusters.

A very interesting result is that similar structural arrangements for the same number of atoms but different total charge exhibit considerably different topologies of the electron densities, this is a consequence of different number of electrons being accommodated for different charge numbers in the same geometry. As a typical example, Fig. 14 illustrates the changes in the number and disposition of critical points for the D_{5h} geometries in Li^q_7 clusters.

Covalent character and cooperativity

In Fig. 18 the degree of covalent character $\mathscr{H}$ ($\mathbf{r}_b$) from Eq. 2 is plotted against the bond–path length (BPL) for the most stable structures for neutral and charged lithium clusters. Li^-_7 consists of Li···NNA interactions in a tight cluster with BPLs of length 5.8 au. The most stable structure of the anionic clusters with nine lithium nuclei also contains Li···NNA interactions for BPLs of 5.0–6.5 au. All of the Li···NNA interactions in this study were found to possess a degree of covalent character. For the $Li^q_{5,6,7}$ clusters the degree of covalent character for the most covalent of each cluster charge and size is seen to be cationic > neutral >

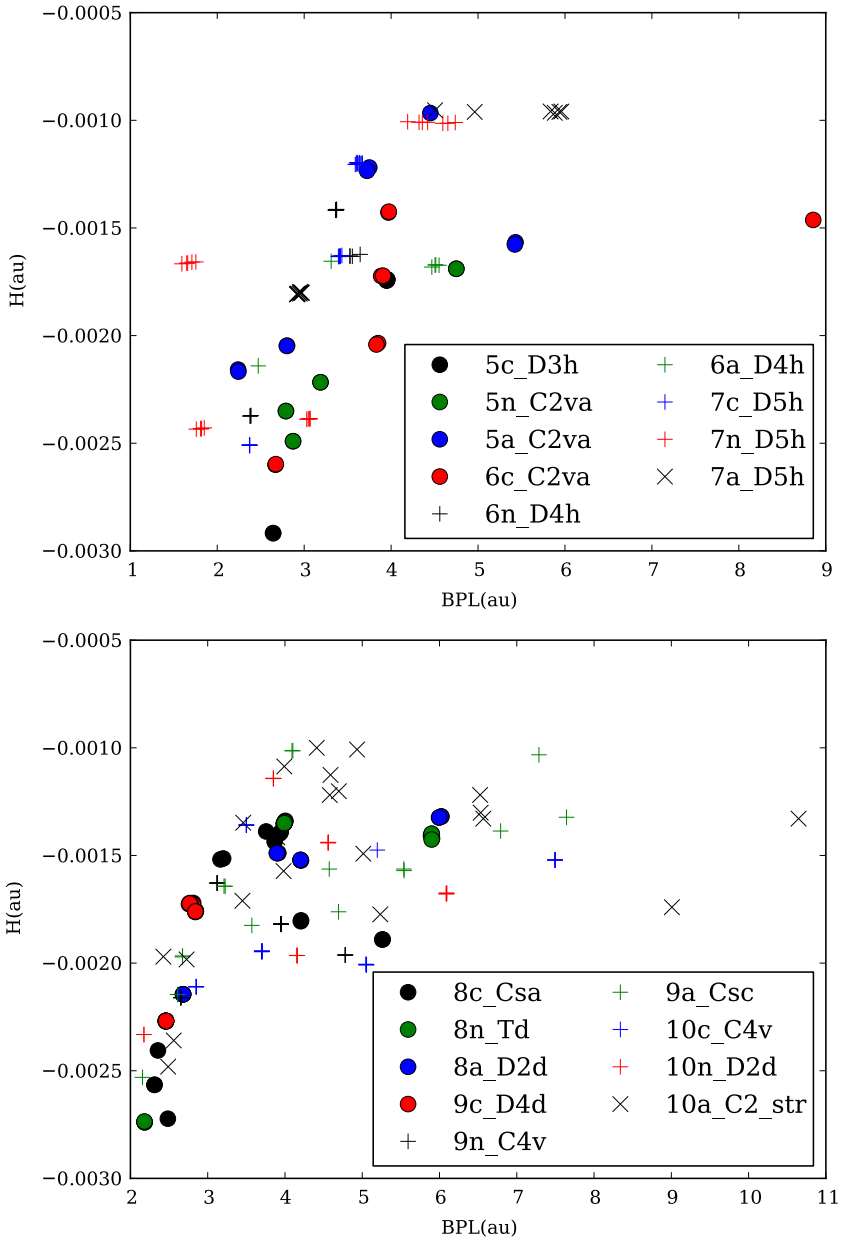

Fig. 18 Variations of the covalent bond character $\mathscr{H}$ ($\mathbf{r}_b$) with BPL for neutral and charged lithium clusters (Eq. 2). Cationic, neutral and anionic clusters are denoted as c, n and a respectively. Top plot refers to clusters having 5, 6 and 7 Li atoms while bottom plot applies to clusters with 8, 9 and 10 Li atoms

anionic and for the cluster size 5>6>7. So the conclusion from Fig. 18 (top) is that smaller cationic clusters tend to posses bonding interactions with a higher degree of covalent character than larger anionic ones. For larger sizes (8–10) the outcome is far less clear, with no distinction between size or charge type on the degree of covalent character present in the bonding interactions.

Conclusions

Eighteen conformational spaces for neutral and charged lithium microclusters ($Li_n^q, n = 5-10, q = 0, \pm 1$) are characterized after random exploration of the corresponding PESs. Very good agreement with available experimental data is obtained. Very complex surfaces are predicted, with the largest structural variety obtained for anionic clusters, for which typical 2:1 ratios in the number of stable conformers when compared to cationic and neutral clusters are predicted for the same number of atoms. Topological analysis of the electron densities suggest that the clusters seem to be stabilized by the presence of non–nuclear attractors located between Li atoms. Approximate gaussian–like radial distributions are obtained for Li···Li distances for all clusters considered in this study. As a general rule, for larger sizes, compact 3D structures are energetically preferred over planar conformations, in addition, increasing the number of atoms by one in the larger clusters seems to also favor structures where new fused tetrahedra are formed. Binding energies per atom predict that cationic clusters are the most

stable when comparing systems having the same number of atoms. Cluster dimensionality obtained from quantum topology instead of the usual means of Euclidean geometry shows a change in geometrical preferences for clusters containing more than seven Li atoms, this observation is also reached (independently) by quantifying the degree of covalency in lithium bonding. A novel scheme of 2D projections of recurrent structural motifs is used to formulate hypothesis about cluster growth.

Acknowledgements This work was partially funded by the University of Antioquia, CODI office. The Hundred Talents Foundation of Hunan Province is gratefully acknowledged for the support of S.J. and S.R.K. This work was made possible by the facilities of the Shared Hierarchical Academic Research Computing Network SHARCNET: www.sharcnet.ca, through the kind auspices of our sponsor Dr P.W. Ayers, Department of Chemistry, McMaster University, Ontario, Canada. Very useful discussions with Professor Pablo Jaque, Universidad Andres Bello, Chile, are acknowledged. D.Y. thanks CONICYT for her PhD fellowship.

References

1. Dugourd P, Rayane D, Labastie P, Vezin B, Chevaleyre J, Broyer M (1992) Chem Phys Lett 197:433
2. Alexandrova A, Boldyrev A, Li X, Sarkas H, Hendricks J, Arnold S, Bowen KJ (2011) Chem Phys 134:044322
3. Benichou E, Antoine R, Rayane D, Vezin B, Dalby FW, Dugourd P, Broyer M, Ristori C, Chandezon F, Huber BA, Rocco JC, Blundell SA, Guet C (1999) Phys Rev A 59:R1
4. Bréchignac C, Busch H, Cahuzac P, Leygnier JJ (1994) Chem Phys 101:6992
5. Alexandrova A, Boldyrev AJ (2005) Chem Theory Comput 1:566
6. Gardet G, Rogemond F, Chermette HJ (1996) Chem Phys 105:9933
7. Sung M, Kawai R, Weare K (1994) Phys Rev Lett 73:3552
8. Rousseau R, Marx D (2000) Chem Eur J 6:2982
9. Rousseau R, Marx D (1997) Pys Rev A 56:617
10. Jones R, Liehtenstein A, Hutter JJ (1997) Chem Phys 106:4566
11. Pérez J, Flórez E, Hadad C, Fuentealba P, Restrepo AJ (2008) Phys Chem A 112:5749
12. Boustani I, Pewerstof W, Fantucci P, Bonačić-Koutecký V, Koutecký J (1987) Phys Rev B 35(18):9437
13. Bonačić-Koutecký V, Fantucci P, Koutecký J (1988) Phys Rev B 37:4369
14. Bonačić-Koutecký V, Fantucci P, Koutecký J (1991) Chem Rev 91:1035
15. Koutecký J, Boustani I, Bonačić-Koutecký V (1990) Int J Quantum Chem 38:149
16. Grassi A, Lombardo G, Angilella G, March N, Pucci RJ (2004) Chem Phys 120:11615
17. Temelso B, Sherrill DJ (2005) Chem Phys 122:064315
18. Wheeler S, Sattelmeyer P, Schleyer R, Schaefer HJ III (2004) Chem Phys 120:4683
19. McAdon M, Goddard W (1985) Phys Rev Lett 55:2563
20. McAdon M, Goddard W (1985) J Non-Cryst Solids 75:149
21. McAdon M, Goddard WJ (1987) Phys Chem 91:2607
22. Fantucci P, Bonaccić-Koutecký V, Jellinek J, Wiechert M, Harrison R, Guest M (1996) Chem Phys Lett 250:47
23. Rousseau R, Marx D (1998) Pys Rev Lett 80:2574
24. Rousseau R, Marx DJ (1999) Chem Pys 111:5091
25. Ishikawa Y, Sugita Y, Nishikawa T, Okamoto Y (2001) Chem Pys Lett 333:199
26. Fantucci P, Polezzo S, Bonačić-Koutecký V, Koutecký J (1990) J Chem Phys 92:6645
27. Koutecký J, Fantucci P (1986) Chem Rev 86:538
28. Bonaccić-Koutecký V, Boustani I, Guest M, Koutecký J (1988) J Chem Phys 89:4861
29. Boustani I, Koutecký JJ (1988) Chem Phys 89:5657
30. Visser S, Alpert Y, Danovich D, Shaik SJ (2000) Phys Chem A 104:11223
31. Blanc J, Bonaccić-Koutecký V, Broyer M, Chevaleyre J, Dugourd P, Koutecký J, Scheuch C, Wolf J, Wöste L (1992) J Chem Phys 96:1793
32. Dougord P, Blanc J, Bonaccić-Koutecký V, Broyer M, Chevaleyre J, Koutecký J, Pittner J, Wolf J, Wöste L (1991) Phys Rev Lett 67 (19):2638
33. Molina L, Alonso JJ (2007) Phys Chem C 111:6668
34. Furche F, Ahlrichs R, Weis P, Jacob C, Gilb S, Bierweiler T, Kappes MJ (2002) Chem Phys 117:6982
35. Gilb S, Weis P, Furche F, Ahlrichs R, Kappes MJ (2002) Chem Phys 116:4094
36. Fernández E, Soler J, Garzón I, Balbás L (2004) Phys Rev B 70:165403
37. Häkkinen H, Moseler M, Landman U (2002) Phys Rev Lett 89:033401
38. Hincapié G, Acelas N, Castaño M, David J, Restrepo AJ (2010) Phys Chem A 114:7809
39. Jenkins S, Restrepo A, David J, Yin D, Kirk S (2011) Phys Chem Chem Phys 13:11644
40. Jellinek J, Srinivas S, Fantucci P (1998) Chem Phys Lett 288:705
41. Bazterra V, Oña O, Caputo M, Ferraro M, Fuentealba P, Facelli J (2004) Phys Rev A 69:053202
42. Tiznado W, Oña O, Bazterra V, Caputo M, Facelli J, Ferraro M, Fuentealba PJ (2005) Chem Phys 123:214302
43. Oña O, Bazterra V, Caputo M, Facelli J, Fuentealba P, Ferraro M (2006) Phys Rev A 73:053203
44. Metropolis N, Rosenbluth A, Rosenbluth M, Teller A, Teller EJ (1953) Chem Phys 21:1087
45. Kirkpatrick S, Gellat C, Vecchi M (1983) Science 220:671
46. Aarts E, Laarhoven H (1987) Simulated annealing: theory and applications. Springer, New York
47. Pérez J, Hadad C, Restrepo A (2008) Int J Quantum Chem 108:1653
48. Pérez J, Restrepo A (2008) ASCEC V–02: Annealing Simulado con Energía Cuántica. Property, development and implementation: Grupo de Química–Física Teórica, Instituto de Química, Universidad de Antioquia: Medellín, Colombia
49. Restrepo A, Mari F, Gonzalez C, Marquez M (1995) Química Actualidad y Futuro 5:101
50. David J, Guerra D, Hadad C, Restrepo AJ (2010) Phys Chem A 114:10726
51. Ramírez F, Hadad C, Guerra D, David J, Restrepo A (2011) Chem Phys Lett 507:229
52. Murillo J, David J, Restrepo A (2010) Phys Chem Chem Phys 12:10963
53. David J, Guerra D, Restrepo AJ (2009) Phys Chem A 113:10167
54. Romero J, Reyes A, David J (2011) Restrepo Phys Chem Chem Phys 13:15264
55. Gaussian 03, Revision E.01, Frisch MJ, Trucks GW, Schlegel HB, Scuseria GE, Robb MA, Cheeseman JR, Montgomery JA Jr, Vreven T, Kudin KN, Burant JC, Millam JM, Iyengar SS, Tomasi J, Barone V, Mennucci B, Cossi M, Scalmani G, Rega N, Petersson GA, Nakatsuji H, Hada M, Ehara M, Toyota K, Fukuda R, Hasegawa J, Ishida M, Nakajima T, Honda Y, Kitao O, Nakai H, Klene M, Li X, Knox JE, Hratchian HP Cross JB, Bakken V, Adamo C, Jaramillo J, Gomperts R, Stratmann RE, Yazyev O,

Austin AJ, Cammi R, Pomelli C, Ochterski JW, Ayala PY, Morokuma K, Voth GA, Salvador P, Dannenberg JJ, Zakrzewski VG, Dapprich S, Daniels AD, Strain MC, Farkas O, Malick DK, Rabuck AD, Raghavachari K, Foresman JB, Ortiz JV, Cui Q, Baboul AG, Clifford S, Cioslowski J, Stefanov BB, Liu G, Liashenko A, Piskorz P, Komaromi I, Martin RL, Fox DJ, Keith T, Al–Laham MA, Peng CY, Nanayakkara A, Challacombe M, Gill PMW, Johnson B, Chen W, Wong MW, Gonzalez C, Pople JA (2004) Gaussian, Inc., Wallingford, CT

56. Bader R (1994) Atoms in molecules: a quantum theory. Clarendon, Oxford
57. Cremer D, Kraka E (1984) Croat Chem Acta 57:1250
58. Jenkins S, Morrison I (2000) Chem Phys Lett 317:97
59. Issacs E, Shukla A, Platzman P, Hamann D, Barbiellini B, Tulk C (1999) Phys Rev Lett 82:600
60. Keith T (2010) AIMALL (Version 10.09.12), aim.tkgristmill.com
61. Tornaghi E, Cooper D, Gerrat J, Raimondi M, Sironi MJ (1992) Mol Sruc Theochem 259:383
62. Cao W, Gatti C, MacDougall P, Bader R (1987) Chem Phys Lett 141:380
63. Platts J, Overgaard J, Jones C, Iversen B, Stasch AJ (2011) Phys Chem A 115:194
64. Glaser R, Waldron R, Wiberg KJ (1990) Phys Chem 94:73
65. Madsen G, Blaha P, Schwarz KJ (2002) Chem Phys 117:8030
66. Bersuker I (2010) The Jahn–Teller Effect. Cambridge University Press, Cambridge
67. David J, Guerra D, Restrepo A (2011) Inorg Chem 50(4):1480
68. David J, Fuentealba P, Restrepo A (2008) Chem Phys Lett 457: 42
69. Zeng T, Fedorov D, Schmidt M, Klobukowski MJ (2011) Chem Theory Comput 7:2864